

## **Chapter 1 Introduction and Literature Study**

### ***1.1 Introduction***

Turbomachinery are critical to various processes and their applications range from micro-turbines to steam turbines and aircraft turbines. Possessing large amounts of kinetic energy, the failure of industrial turbine blades during operation are typically quite severe with regards to subsequent secondary damage. In the recent past, a single blade failure on a steam turbine rotor resulted in the destruction of the entire turbo-generator train leading to a large financial loss (Spicer, 2003a; Spicer, 2003b). It is therefore of great importance to monitor the health of turbomachinery on-line in order to ensure the long term health and availability of these machines.

To monitor blade health in an on-line fashion, it is useful to obtain on-line blade vibration information. Various techniques exist to accomplish this, the two most common techniques using blade strain and blade tip Time-Of-Arrival (TOA) signals respectively. Strain gauges are however limited in life span due to the harsh operating environment whereas a large number of sensors are required to obtain sufficient measurement bandwidths when the TOA technique is implemented. Sufficient sensor life span as well as measurement bandwidth are required for long term, accurate blade condition monitoring. For this reason, laser Doppler vibrometry is a very promising measurement technique. Specifically, Eulerian Laser Doppler Vibrometry (ELDV) enables the high bandwidth vibration measurement of an entire row of blades using a single sensor. It is this technique that this thesis is concerned with, focussing on its application to the condition monitoring of free standing axial-flow rotor blades.

ELDV involves the laser beam being focussed at a fixed point in space and measurements are available for the short periods during which the rotor blades sweep through the beam. Since these sample periods are at most inversely proportional to the Blade Pass Frequency (BPF), frequency domain information is available only for a frequency resolution equal to the BPF using conventional signal processing techniques. This disqualifies these signal processing techniques for useful information pertaining to blade condition monitoring. In order to obtain useful information, Non-Harmonic Fourier Analysis (NHFA) is employed.

The thesis is divided into five chapters. The first chapter contains a literature study focussing on topics such as the causes and influences of blade vibration as well as blade failure modes. Several damage detection parameters are also considered along with different on-line blade vibration measurement techniques and systems.

Thereafter some modelling and experimental testing issues are investigated as well as practical issues with regards to laser Doppler vibrometry. Different signal processing techniques are also considered.

The second chapter deals with an analytical study of the ELDV technique applied to a traversing and vibrating cantilever beam using the Euler-Bernoulli continuous beam formulation. The results are verified experimentally after which an approach is formulated for simulating ELDV numerically in a Finite Element Model (FEM) environment.

Chapter 3 presents results from experimental ELDV and Tracking Laser Doppler Vibrometry (TLDV) testing on a single-blade test rotor at a single rotor speed. Incremental damage is induced in the blade and it is shown that Maximum Absolute Unwrapped Phase Angle Trends (MAUPATs) from NHFA around various reference frequencies are good indicators of blade health deterioration. The results are verified numerically.

The next chapter presents experimental ELDV and TLDV results obtained from a multi-blade rotor at different rotor speeds. Considering various damage cases on multiple blades, Artificial Neural Networks (ANNs) are successfully trained on the statistical properties of MAUPATs as well as two time domain parameter trends. It is shown that measurements from multiple ELDV measurement positions are advantageous.

Chapter 5 presents the conclusions reached in this thesis and proposes work for further studies.

## **1.2 Blade vibration**

### **1.2.1 Operational blade excitation**

Turbine blades are predominantly subjected to periodic nozzle excitation distributed along the blade lengths (Rao and Vyas, 1985; Irretier, 1988; Rieger, 1988). The load on a rotating blade can thus be described as a Fourier-series, the various harmonic coefficients of which are affected by the unevenness of the nozzle spacing as well as partial (i.e. uneven) steam admission. Rao and Vyas (1985) consider three components of the forcing function namely in the rotor-axial and tangential directions as well as a moment acting on the blade.

Additional blade forces result from flow instabilities (Gadala and Byrne, 1986). The flow instabilities are manifested as white random noise, resulting in the excitation of blade natural frequencies.

Ziegler (1994) groups operational blade vibration into resonance, stochastic response and flutter. Resonance vibration occurs when one of the blade natural frequencies coincides with one of the harmonics of rotation speed whereas stochastic vibration is a result of stochastic flow excitation. Ziegler attributes flutter to the coupling of blade natural vibration modes and flow forces.

Kielb and Abhari (2003) present a report of the independent and simultaneous structural and aerodynamic damping effects in a single stage High Pressure (HP) turbine disk at engine-level rotation speeds. According to these two authors, damping in a turbine is one of the most important factors influencing blade forced response and flutter. They identify the three major sources of damping in a rotating blade as material damping (which they state to be negligible), structural damping and aerodynamic damping. Performing tests on the HP turbine disk at different conditions using blade-mounted strain gauges as transducers and blade-mounted piezoelectric actuators, Kielb and Abhari (2003) reach a number of important conclusions. A very interesting observation is that structural damping in the turbine disk decreases as rotation speed increases. The authors attribute this phenomenon to the fact that as the centrifugal load on a rotating blade increases, energy dissipation as a result of friction between the blade/hub interface decreases. Kielb and his co-worker also conclude that aerodynamic damping forms a major part of total blade damping during rotation.

### **1.2.2 Rotational effects**

The most intuitive effect of rotation on a structure is that of rotational stiffening as a result of centrifugal forces. From experimentation on a single-blade rotor, Fan et al. (1994) note that rotational stiffening causes the blade natural frequencies to increase in a nonlinear way, since the blade centrifugal force is proportional to the square of the rotation speed.

Rotating structures are furthermore subjected to additional forces including gyroscopic forces, rotor-stator rub forces, electromagnetic forces, unsteady aerodynamic forces and time-varying fluid forces (Ewins, 2000:80). All of these forces can destroy the symmetry of the rotor system matrices pertaining to the system equations of motion. Being velocity-dependent, gyroscopic effects introduce a skew-

symmetric component in the damping matrix of the system. Gyroscopic forces furthermore cause the natural frequencies of the rotor to be dependent on rotation speed. These frequencies either increase or decrease with speed, depending on whether the corresponding mode shape is a forward or backward whirl mode.

Rao and Sreenivas (2003) state that the forward whirl mode is furthermore affected by centrifugal stiffening effects, whereas the backward whirl mode is additionally influenced by spin softening. Spin softening is another rotational phenomenon where the rotor stiffness matrix becomes speed-dependent (Nikolic et al., 2007).

Sreenivasamurthy and Ramamurti (1981) numerically investigate the Coriolis effect on the vibration of a single rotating blade. In their investigation, the authors include rotational stiffening effects. By varying the rotation speed, stagger angle and aspect ratio of the blade, the influence of the Coriolis effect is observed to change. The authors observe that the Coriolis effect causes the first flapwise blade frequency to decrease as rotation speed increases. Furthermore, the blade aspect ratio determines whether the first torsional blade frequency increase or decrease due to Coriolis acceleration. The authors also found the blade stagger angle to largely influence the extent of the Coriolis effect on the blade frequencies. The authors conclude their article in stating that in general, the Coriolis effect can be ignored for cases where the first blade bending frequency is higher than the rotation frequency. However when the rotation frequency is very high and also higher than the first blade natural frequency, it is recommended to include Coriolis effects.

### **1.2.3 Blade manufacturing tolerances**

#### **1.2.3.1 Blade roots**

Singh (1998) discusses the effects of dimensional tolerance of blade roots on the maximum stresses in the blade roots. The dimensional tolerance considered by the author is the gap between the blade root attachment and the supporting structure or rotor. Results show that the maximum stress in a blade root increases as the gap increases. Since blades can be considered as cantilever beams, which means that their dynamic responses is very sensitive to their individual boundary conditions, this factor will influence the blade vibration responses, as confirmed by Bhat et al. (1996).

Orsagh and Roemer (2002) state that connection stiffness within blade-root interfaces and blade-tiewire interfaces, centrifugal effects and thermal effects influence the accuracy and effectiveness of modal test data taken from bladed disk assemblies. The

authors note that differences in measured frequencies of substructures such as blade groups can be anticipated due to dimensional tolerances, manufacturing defects, material processing and installation procedures. The effect of these differences is manifested as scatter of natural frequencies about a mean value. According to the authors, scatter of 5% is normally considered acceptable among the manufacturing community for Low Pressure (LP) steam turbine blades. Orsagh and Roemer note that if an assembly is tested with blade fixity problems such as loose blade-root interfaces (which is an example of dimensional tolerance), the bladed disc natural frequencies will be lower than for rigidly fixed blades. Looseness will also create structural nonlinearities. However according to them, blade-root looseness is eliminated by centrifugal forces during operation to ensure tight blade-root interface fits, making blade and disk essentially an integral structure.

Bhat et al. (1996) also note that due to manufacturing tolerances, some variation can occur with regards to blade natural frequencies of a turbine. Impact test measurements were taken on blades of two stages of a LP turbine of a 235 MW turbo-generator set. Some scatter was observed in these measurements with bands of 76-85 Hz, 125-140 Hz and 155-170 Hz for the first three modes. The authors note that the scatter is probably due to non-uniformity in root fixity and aerofoil cross-section.

### **1.2.3.2 Mistuning**

Afolabi (1988) discusses the modal characteristics of turbomachinery blades in multi-stage rotors. He investigates the effect of inter-stage coupling on the modal characteristics of turbine blades. The author refers to experiments showing that the vibration characteristics of an isolated blade differ a lot from blades of bladed disc assemblies: When a number of identical blades are assembled on a common disc, the previously isolated blade modes are transformed into spectral bands of groups of the same number of modes. Most of these modes are double modes. It is further noted by Afolabi that all the blades within an assembly are not identical due to manufacturing tolerances and are referred to as being mistuned. Although the resulting differences between blades are very small, the effects of mistuning cannot be ignored when coupling (as provided by the blade disc) exists among the blades. If there is mistuning involved among the blades in the assembly, there is a change in the modal characteristics. This has the effect of the system having very high modal densities within the spectral bands. Resulting uneven distribution of blade amplitudes of a given mode shape may cause some blades to possibly fail prematurely due to the high amplitudes of such blades.

Hollkamp and Gordon (2001) give an in-depth discussion on the topic of bladed disc modal analysis and concur on a number of Afolabi's findings. They note that periodic structures are "notoriously sensitive" to mistuning. A number of difficulties are involved with bladed disc modal analysis. Also, multiple inputs and high-resolution techniques are required to separate repeated modes. Thus these structures have multiple closely spaced frequencies, making the task of mode shape estimation extremely difficult. They state that slight variations in blades mistune individual blade natural frequencies and affect the entire system.

### ***1.3 Blade damage and failure modes***

Rieger (1988) discusses several important blade failure types and their causes pertaining to steam turbines. The author notes that from electrical utility records it is shown that approximately 30% of all steam turbine forced outages can be attributed to blade problems (Rieger, 1988:453). According to the author there are four aspects that influence the life span of a blade. Two of these relate to the magnitudes and distributions of steady mean and alternating stresses. According to Rieger (1988:455) both of these have maximum values at certain locations such as among others, the blade root-disk attachment region. Mathwin (2004) confirms this in stating that cracking in steam turbine blades with fir-tree roots mostly occurs in the region of the roots' top serration. Further literature sources (Gadala and Byrne, 1986; Mazur et al., 2008) also refer to incidents involving the failure of LP turbine blades as a result of crack growth at the blade-root top serration.

Rieger (1988) notes that at each of the locations he mentions, the mean stress value depends on centrifugal and steam loading conditions. Visser (2004) also refers to centrifugal loading as being one of the greatest influences on blade fatigue life. According to Rieger (1988:455) alternating stresses in turbine blades result from dynamic steam stimuli and the corresponding modal response from the entire blade group involved.

Another influence of great importance is the effect of thermal stresses (Visser, 2004; Boutarek et al., 2008). This relates mainly to the rates of heating up and cooling down of turbine blades during run-ups and run-downs respectively.

A large number of possible crack initiation and failure mechanisms pertaining to turbomachinery blades exist. The following sub-sections highlight some of the more predominant mechanisms.

### **1.3.1 Fatigue**

Fatigue in turbine blades is classified as either High Cycle Fatigue (HCF) or Low Cycle Fatigue (LCF) (Rieger, 1988:456). HCF is normally associated with high mean stress levels and moderate dynamic stresses whereas LCF is associated with fewer load cycles of much larger strain ranges. LCF is furthermore frequently associated with corrosion or high temperature. Possible causes of fatigue listed by Rieger (1988:481) are unsymmetrical stage steam flow, nozzle wake excitation resonance, partial admission of steam, torsional transients, generator electrical faults and excessive condenser pressures.

According to Bhat et al. (1996), the main cause of turbine blade failure is vibration-related fatigue. Although turbine blades are designed to have natural frequencies not coinciding with operational frequencies, they still experience resonance excitation during run-up and run-down of the turbine.

Fatigue can furthermore be exacerbated by other factors. Corrosion assisted fatigue is “probably the major source of steam turbine blade fatigue failures” according to Rieger (1988) and confirmed by Beaumont (2004). Rieger (1988:459) notes that corrosion assisted fatigue may occur where large dynamic stresses applied with high steady stress are present in a corrosive environment.

In aero-engines, the interaction of both creep and fatigue mechanisms is one of the main causes of blade failure (Infante et al., 2009).

### **1.3.2 Stress-corrosion**

The mechanism of stress-corrosion is a combination of dynamic stress and a corrosive medium (Boutarek et al., 2008; Rieger, 1988). Rieger (1988:458) does however note that the presence of dynamic stress is not necessarily a requirement for the occurrence of a stress-corrosion failure. According to Beaumont (2004), Stress-Corrosion Cracking (SCC) usually occurs in steam turbine blades of low alloy materials in a wet steam environment at elevated temperatures. Beaumont notes that SCC can occur even when the steam has good chemical qualities.

### 1.3.3 Foreign object damage

Foreign Object Damage (FOD) occurs when a foreign object impacts a blade during operation. According to Tappert et al. (2001:3287) such an impact momentarily affects the particular blade's vibration, resulting in transient vibration of the blade. Depending on the magnitude of the impact, plastic deformation of the blade may also occur.

Infante et al. (2009) note that FOD due to the impact of small debris results in blade "nicking". These "nicks" then act as stress raisers, which are prone to crack initiation. They furthermore state that FOD tends to compromise the rotor mechanical balance which may lead to aerodynamically induced blade flutter.

### 1.3.4 Flutter

According to King et al. (2006), blade flutter is a self-excited dynamic instability that may, among others, arise from cracked or damaged blades. It manifests itself as an acoustic phenomenon and as a result may not propagate through the turbine support structure. Traditional monitoring methods such as bearing vibration monitoring may as a result not be sufficient for detecting blade flutter.

Mazur et al. (2006) report on the failure of a number of last-stage LP turbine blades of a geothermal unit. The main contributor to the HCF failure of the blades was identified as unstable flow excitation or stall flutter. They state that flow-induced blade oscillations are in general more prominent in the last 10% of the blade length. They also note that aeroelasticity phenomena with largely increased vibratory stresses in blades can occur while operating the turbine at low load/ low vacuum conditions.

In another paper, Mazur et al. (2008) investigate the failure of last stage LP turbine blades of two 660 MW units. Again one of the main contributors the HCF failure of the blades was flutter that occurred at low load/ low vacuum operational conditions.

### 1.3.5 Transient load events

Mazur et al. (2008) studied the failure of last stage LP turbine blades. They note that transient load events on the generator due to other sudden transient events on the electricity grid induced transient torsional vibrations of the rotor. This in turn excited the first tangential mode shape of the blades, resulting in high quantities of cycles of high vibratory stresses in the blades.

## **1.4 Blade health indicators**

### **1.4.1 Natural frequencies**

Wu and Huang (1998) consider the vibration of a cracked rotating blade. They consider a single rotating blade that is mathematically modelled as an Euler's beam with constant cross section. Only transverse bending deflection is considered in the paper. The equations of motion were derived by the authors by looking at crack-released energy in conjunction with weighted residuals. Wu and Huang focussed on the effect of crack size and location on the first four natural frequencies of the modelled blade. From their test results, the authors draw a number of conclusions. Firstly, they conclude that the dynamic characteristics of the rotating blade are significantly influenced by the location of the crack. The effect of this is that the sensitivity of blade natural frequency shift to damage increases as the crack is located closer to the blade root. This is Wu and Huang's (1998) second conclusion along with the fact that at some locations for specific modes, the natural frequency is unchanged. They call these locations inflection points, which are more commonly known as nodal points. Their third conclusion is that as the crack depth increases, the natural frequencies decrease. Wu and Huang (1998) finally conclude that natural frequencies and deflective responses of blades are potential indices for crack identification. They advise that in order to develop a sophisticated on-line crack detection technique, quantitative studies of these indices must be studied. In other words, the relationship between crack severity and its effect on blade natural frequencies and deflections need to be established in order to develop such a system.

Yang et al. (2006) show experimentally that decrease in natural frequencies of a turbine blade is related to damage. Their aim was to determine whether damage in a blade could cause sufficient decrease in any natural frequency of the blade for that natural frequency to be close to resonance. The authors experimentally and numerically performed tests on a single clamped blade of the tenth stage of a nuclear power station LP turbine. They induced damage close to the blade root in the form of a crack in a controlled manner, each level for which they performed a modal analysis on the blade.

Kumar et al. (2007) consider the on-line damage detection of rotating turbine blades. From strain energy and kinetic energy equations of a rotating Timoshenko beam with taper and twist, they consider the reduction in a specific frequency of a rotating blade as a health residual which can be tracked for purposes of condition monitoring. The

authors go on to discuss the use of thresholds to make the damage detection technique using the residual more robust.

Maynard et al. (2001) focus on the use of shaft torsional measurements to monitor changes in global blade natural frequencies for damage detection.

### **1.4.2 Damping**

Ziegler (1994) states that the “damping constant” relating to blade vibration is dependent on operational variables such as friction between blade and flow medium and excitation force amplitude. It is also dependent on the blade’s material damping but more importantly on the friction between the blade root and the shaft, implying its feasibility as use of a blade damage indicator. Ziegler does however note that determining this parameter from in-service measurements is not straightforward.

Von Flotow et al. (2000) state that damping may be a possible blade damage indicator.

### **1.4.3 Amplitude**

Wu and Huang (1998) state that vibration response amplitudes are affected by damage. Von Flotow et al. (2000) also consider vibration amplitude changes as a possible blade damage indicator.

King et al. (2006) consider the amplitude of rotor tracked orders to be indicative of among others, blade damage.

### **1.4.4 Phase angle**

Changes in natural frequencies, mode shapes and damping values only become noticeable at high damage levels (Hueck, 2004; Jacobs and De Roeck, 2003). One parameter that is a very sensitive damage indicator is vibratory phase angle change, as shown by Jacobs and De Roeck (2003) from dynamic testing on a stationary concrete beam. In comparison with the abovementioned parameters, Jacobs and De Roeck find phase angles to already show significant changes at low damage levels. With regards to rotating blades, the sensitivity of the natural frequency shift to damage in a blade decreases with an increase in rotor speed (Wu and Huang, 1998; Yang et al., 2006). This makes vibratory phase angle change a promising damage indicator for rotating blades.

According to King et al. (2006) the monitoring of the phase and amplitude of a tracked engine order from shaft vibrations can also provide information on crack propagation in turbine blades.

#### **1.4.5 Operational modal analysis**

Various literature sources deal with using modal analysis to identify damage in a structure. Modal analysis seeks to characterise a mechanical system in terms of its various vibration modes. In classical modal analysis, measured responses to known input forces render the Frequency Response Functions (FRFs) for this purpose. However in operating machinery (especially turbines) it is difficult to measure all the input forces and hence it is necessary to estimate the modal parameters by other means.

Cauberghe et al. (2003) present the Combined Non-Linear Least Squares Frequency Method On Input Output Spectra (CLSF-IO) to estimate modal parameters from output-only data. The Gauss-Newton method is used to solve the non-linear optimization problem. Cauberghe and his co-authors also briefly draw a comparison between the CLSF-IO method and the Auto Regressive Moving Average (ARMA) method in terms of unknown force estimation.

Shen et al. (2003) review the theoretical aspects of the Natural Excitation Technique (NExT) and also present a frequency domain poly-reference scheme for modal identification using Power Spectral Density (PSD) and cross spectral density functions.

Simani (2005:204) and Brincker et al. (1996:3) refer to a number of order selection indicators. These include the Final Prediction Error (FPE), Akaike Information Criterion (AIC), Minimum Description Length (MDL) and Predicted Percent Reconstruction Error (PPCRE). FPE presents a trade-off between residue variance and model parameter number according to Brincker et al. (1996). Brincker and his co-workers select an ARMA model for an offshore platform based on the lowest FPE.

### **1.5 Blade vibration measurement techniques**

Al-Bedoor (2002) classifies blade vibration measurement techniques as direct or indirect, referring to the transmission path between sensor and blade. What makes

direct techniques attractive is that the transmission path is minimal, thereby reducing signal noise pollution.

### 1.5.1 Strain gauges

The traditional and popular method of measuring blade vibrations involves strain gauges installed on individual blades. The advantage of this method is that individual blade vibration measurements can be performed over an entire revolution of the rotor. However, this method also has quite a number of drawbacks.

1. Sensor life span

Kadoya et al. (1995:486) highlight a number of factors reducing the life span of strain gauges operating in steam environments. These include high centrifugal forces and high temperature. Another influence is of course erosion (Al-Bedoor, 2002).

2. Signal transmission

Transmission of signals from the strain gauges is perhaps the biggest problem associated with the technique. Slip ring assemblies can be used for this purpose, although these present their own problems in terms of life span due to wear as well as installation problems on a large rotor such as a steam turbine. Signal transmission can also be accomplished with radio-telemetry systems, although they are costly and time consuming to set up (Beuseroy and Lengelle, 2007). Due to the presence of rotor seals, grooves furthermore need to be machined in the shaft in order to accommodate the wires leading from the strain gauges (Gloger, 1988:2; Kadoya et al., 1995:486; Fangman et al., 1967:21A).

3. Number of sensors

The number of sensors that need to be installed to monitor a single turbine rotor stage is large. However, Oberholster and Heyns (2006) show that damage detection on a rotor can be accomplished using less than one sensor per blade by exploiting the blade global mode shapes phenomenon.

4. Rotor interference

Beuseroy and Lengelle (2007) state that strain gauge instrumentation often interferes with the aerodynamic and mechanical properties of the rotor of concern.

### 1.5.2 Blade tip TOA

Blade tip TOA is a non-contact blade vibration measurement technique. This technique utilizes a number of stationary probes mounted on the enclosure of a

specific blade row. The probes sense the proximity of passing blades, which makes it possible to measure the times at which each blade tip passes one of the probes. A once per revolution shaft speed sensor is used for the purpose of relating these signals to designated blade numbers (Zielinski and Ziller, 2000:847). Figure 1 shows a typical system setup consisting of two proximity probes and a shaft speed sensor.

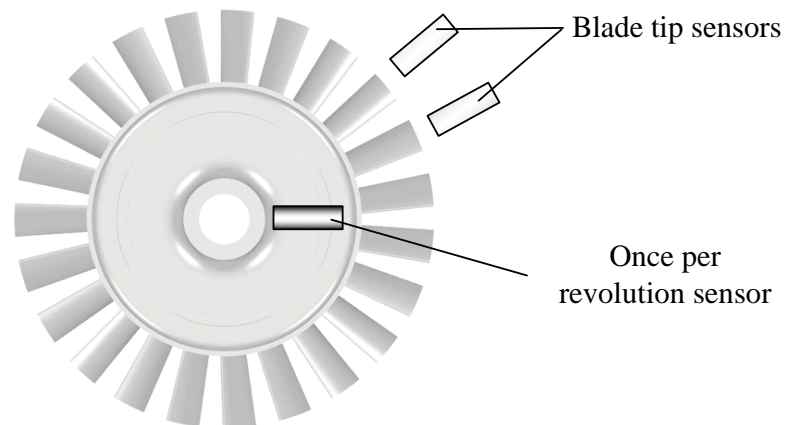


**Figure 1: Typical blade tip TOA measurement system setup**

Drawing an analogy of a TOA system to a signal processing frame of reference, such a system can be seen as an “optical” Analogue to Digital Converter (ADC) of blade position. Another analogy can be drawn to that of a shaft encoder: Taking measurements utilizing a shaft encoder can be seen as taking TOA measurements on blades with zero lengths.

According to Zielinski and Ziller (2000:853) the shape and magnitude of a resonance curve measured using TOA, is influenced by the exciting engine order, the circumferential position of the probes as well as their spacing.

Beuseroy and Lengellé (2007) introduce a system consisting of a number of individual groups of regularly spaced optical probes for TOA measurements. By simultaneously sampling the signal using different sampling frequencies (as a result of different probe spacing for each group) they are able to analyze multi-component blade vibration signals over a wide frequency bandwidth. According to Beuseroy and Lengellé (2007) the limitation of typical TOA systems is the analysis of blade vibration at only a single frequency. Using two groups of probes, the authors give the following relation to the maximum dynamic range of measurement:

$$\text{Dynamic range} = \frac{g_1 \cdot g_2}{2} \psi$$

**Equation 1**

with  $g_1$  and  $g_2$  the number of probes in each respective group of sensors and  $\psi$  the rotation frequency of the rotor. This implies a large number of probes if a high bandwidth is required at especially low rotation speeds, a shortcoming of TOA that is also implied by Watkins and Chi (1989).

Heath and Imregun (1998) go further to state that this may lead to an impractical number of probes in terms of installation costs. This forces the use of a low number of sensors that in turn necessitates indirect amplitude and frequency extraction techniques from the data. As a result one of the drawbacks of the TOA technique is that the interpretation of the TOA signals is complicated.

### **1.5.2.1 Probe Types**

Zielinski and Ziller (2000) compare optical probes and capacitive probes as sensors and note that the latter are inferior to the former in terms of amplitude resolution and as a result also Signal to Noise Ratio (SNR).

Drumm and Haase (2000) state that light cannot easily be used to measure blade tip clearance or radial vibration (note that the authors are not referring to laser light here). In comparison to capacitive probes, they discuss a number of shortcomings of light probes. One of these is the fact that light probes tend to be bulky. This makes it difficult to place a number of probes in close proximity of each other, which in turn limits the measurement bandwidth of the system. On the other hand, multiple capacitive probes can be closely spaced. According to the two authors, a substantial problem with light is contamination from debris that blocks the light. Although contamination has an effect on the tip clearance measurements by a capacitive sensor, there is no effect on the TOA measurement. Another problem with light probes is their operating temperature limit. According to Drumm and Haase (2000), capacitive sensors can be made for very high temperature applications. With regards to the SNR as mentioned by Zielinski and Ziller (2000), Drumm and Haase refer to the HiBand system from ExSell instruments. This system makes use of a Direct Current (DC) biasing technique in the probe amplifier to overcome this problem.

Kadoya et al. (1995) focus on the blade tip TOA measurement application of laser probes. Aono et al. (1985) make use of laser probes due to their good frequency characteristics in comparison to inductive and capacitive probes.

### 1.5.2.2 Aliasing

Zielinski and Ziller (2000:849) note that aliasing occurs in a TOA system because the most blade vibration frequencies are above the Nyquist frequency ( $f_{NQ}$ ) given as:

$$f_{NQ} = \frac{f_s}{2} = \frac{g\psi}{2}$$

**Equation 2**

with  $f_s$  being the sampling frequency and  $g$  the number of circumferentially equally spaced probes.

Balda (2000:680) gives the equation for calculating an aliased frequency ( $f_{aliased}$ ) as:

$$f_{aliased} = f_{actual} - f_s \cdot \text{round}\left(\frac{f_{actual}}{f_s}\right)$$

**Equation 3**

with  $f_{actual}$  being the actual frequency that is aliased.

A problem occurs when  $f_{actual}$  is an integer multiple of  $f_s$  as this will result in  $f_{aliased}$  being zero. This means that the specific frequency will not be visible in the spectrum. This will not necessarily be a cause of concern during running up or running down of a turbine, as the aliased frequency can be tracked as a zigzag line in waterfall plots of the measured spectra (Zielinski and Ziller, 2000:849). This is because the sampling frequency varies with the shaft rotation speed and as a result, the aliased frequency also varies as can be concluded from Equation 3. However it may present a problem when this occurs at a steady operating speed. But according to Balda (2000:681) estimates of the resonance frequencies are available from the blade manufacturers, which mean that the TOA system can be designed accordingly.

### 1.5.2.3 Probe configuration

Zielinski and Ziller (2000) discuss the capabilities of different probe configurations. One of the main considerations with regards to selecting the number of probes relates to aliasing as discussed in Section 1.5.2.2. For three probes, engine order multiples of 3 will not be visible while as for five probes, all engine order multiples of 5 will be invisible. The authors note a shortcoming of using three probes which is that the

measured amplitude of the first torsional blade mode is about 20% smaller than what it actually is. They attribute this to the radial displacement of the rotor axis at higher speeds. Speed-synchronous vibrations can be measured using two probes only with the requirement that “the resonances must be traversed completely (Zielinski and Ziller, 2000:852). A single or average spectrum of all the blades can be obtained using a single probe as well. The assumption here is that all the blades are vibrating at the same amplitude and with a “fixed interblade phase difference” (Zielinski and Ziller, 2000:854). The authors mention in their conclusion that using four probes, comprehensive data on all speed-synchronous vibrations can be obtained.

#### **1.5.2.4 Assumptions**

Zielinski and Ziller (2000:848) make the same assumptions that blade tip motion caused by vibration is much slower than that caused by rotation, and that these vibrations are moderately damped. They also ignore any interactions among blades.

#### **1.5.2.5 Signal processing**

One of the practical issues of using a proximity probe in TOA measurements is to choose the thresholds that will define when a blade has arrived at and passed a sensor (Newby, 2004). Zielinski and Ziller (2000:848) advise to make use of what they call “constant fraction triggering” on the falling edge of a signal measured with a capacitive probe to define the time of a blade passing the sensor. They note that this is necessary to make the trigger timing largely independent of signal amplitude, which varies with tip clearance.

#### **1.5.3 Pressure signals**

Aretakis et al. (1998) use computational fluid dynamics calculations to derive unsteady pressure signals of blade tips sensed by a stationary transducer. These signals are then used to identify certain blade faults. The paper focuses on typical blade damage as a result of FOD. It does not seem that the authors considered blade vibration as part of their signal derivations. Aretakis and his co-workers make use of what they call "enveloping" of the power spectra of the pressure signals for signal classification. Basically what this means is that they use only the values of multiples of rotation speed for classification. Using ANNs, the authors are able to discern between different faults very successfully. In essence, what Aretakis et al. (1998) describe is a variation on blade tip TOA systems.

#### **1.5.4 Shaft torsional vibration measurements**

Maynard et al. (2001) performed an investigation into the feasibility of detecting cracks in gas turbine blades using torsional shaft vibration measurements. They use a 60-tooth shaft encoder installed on the HP turbine disk of a jet engine to obtain measurements. From the results of this investigation, the authors note that there is high confidence in the practical applicability of this technique. From the paper, it seems that Maynard and his co-authors used only a single probe to obtain measurements from the shaft encoder.

#### **1.5.5 Audio signals**

King et al. (2006) discuss the application of time-frequency analysis to a microphone signal for the purpose of aero gas turbine condition monitoring. Using this type of analysis, FOD as well as blade flutter can be detected. This type of monitoring can be useful as blade flutter may arise from cracked or damaged blades.

#### **1.5.6 Fibre Bragg Grating sensors**

Hwang et al. (2006) present a new monitoring technique using Fibre Bragg Grating (FBG) sensors. An FBG sensor is in essence an optical fibre, which is subjected to a grating process resulting in the fibre having a periodic modulation of refraction index. When broadband light is supplied to the sensor while it is subject to either compressive or tensile stress, the wavelength of the reflected light changes accordingly. This change in wavelength can then be used to measure stress in the sensor. A single optical fibre can consist of a number of FBG sensors, each with a different wavelength reflection characteristic. Hwang and his co-workers propose and test a telemetry-free system with FBG sensors installed on two rotating fan blades. The sensors terminate at the shaft centre (indicating shaft machining) and are supplied with broadband light from a source over a gap distance aligned with the shaft centre. Reflected light from the sensors is then measured at the light source location.

#### **1.5.7 Interferometry**

Interferometry for the purpose of vibration measurements involves an image of a deformed or vibrating structure being superimposed onto a reference image of the same structure. This can be implemented using either Holographic Interferometry (HI) or Electronic Speckle Pattern Interferometry (ESPI).

Caponero et al. (2000) present the theoretical background for both techniques. HI involves recording a holographic image of the structure at time instant  $t$ . The holographic image of the structure at time instant  $t + \Delta t$  is then superimposed onto the recorded holographic image, producing an image with fringes relating to the deformation of the structure. Although this technique does yield high spatial resolution results it is time consuming according to the authors and not suitable for industrial application, as it requires chemical or electrostatic processing of holographic plates.

ESPI however does not require analogue recording media and is thus more feasible for industrial implementation. A reference image of the undeformed structure is recorded along with a reference beam. This yields an image with the reference beam interfering with the speckle field of the structure. The same type of image of the deformed structure is then superimposed on this reference image, again yielding a fringe pattern.

Lesne et al. (1985) use an image de-rotator in order to perform HI on a rotating disk.

### **1.5.8 Laser Doppler velocimetry**

Pfister et al. (2006) present a fibre optic laser Doppler position sensor based on laser Doppler velocimetry for the purpose of blade tip clearance and vibration measurements. Using two laser diodes with different wave lengths, it is possible to simultaneously measure object position and velocity. The authors state that the measurement uncertainty of the sensor is not strongly affected by coherent speckle noise. Although Pfister and his co-authors do not state the maximum sensor measurement bandwidth, they refer to measurements on a rotor with a BPF of 21.7 kHz.

From their references, Lv et al. (2003) seem to implement this technique to measure micro-helicopter blade dynamics. The authors perform signal analysis on the samples using Fast Fourier Transform (FFT) analysis, yielding a very coarse frequency resolution.

### **1.5.9 Laser Doppler Vibrometry**

Laser Doppler Vibrometry (LDV) employs the Doppler effect to measure vibrations on an object. By directing a laser beam onto a target, the reflected light is shifted in

frequency in accordance with the target's vibration velocity. By combining the reflected light with a reference beam, the vibration velocity of the target is obtained.

### **1.5.9.1 Eulerian Laser Doppler Vibrometry**

The ELDV measurement technique involves the LDV being directed at a fixed point in space (Castellini and Santolini, 1998:44). This corresponds to definition of the Eulerian reference frame commonly used in fluid dynamics where the coordinates of the reference frame are fixed and a fluid is observed as it passes by (White, 1999:216). Applied to turbomachinery blades, measurements are then taken as the rotor blades sweep through the laser beam.

Sever (2004) mentions a number of articles dealing with this technique. The earliest of these is by Davis and Kulczyk (1969), who attached reflective tape to the blade to obtain adequate back-scattered light for vibration measurement purposes. Because of the measurement approach the measured signals are available in short pulses. In a later article, Kulczyk and Davis (1970) present some results on using the amplitudes of these pulses to represent vibration of the whole turbine blade row, should the particular frequency of interest be too low to be captured in a single pulse. Davis and Kulczyk (1969) attribute the difficulty of interpretation of the signals to the LDV signal strength.

The same authors (Kulczyk and Davis, 1973) go on to discuss the technique in more detail. According to them, this measurement technique has been used successfully on a turbine with blade tip circumferential velocities of 300 m/s. Kulczyk and Davis note that the short pulse nature of the measured signal affects the output bandwidth and accuracy of the measurement. The authors further state that the measured velocity is not a function of the shape of the blades. Kulczyk and his co-author go on to note that the measured signal is closer to narrowband Gaussian noise than pure-harmonic oscillation, thus limiting the accuracy of the measurements. The authors also give a number of equations to obtain an SNR prediction.

Cookson and Bandyopadhyay (1980) use a laser Doppler fibre optic probe to take axial measurements on rotating blades. The authors use a simple eight-blade test rotor of which one of the blades is excited by a piezo-electric exciter at a fixed frequency. Focussing on only one specific point on the blade width, they develop analytical equations for determining the vibration frequency and amplitude of a single point on the blade for low frequencies. Higher frequency information is attainable when

measurements are taken at slightly different rotation speeds. The equations derived by Cookson and Bandyopadhyay (1980) are however only valid for blade vibration resulting from pure-sinusoidal excitation and not from impulse excitation.

Finke and Schmidt (1996) present a measurement technique similar to that of Cookson and Bandyopadhyay. They make use of the Shannon theorem to obtain blade vibrations. Sampling at frequencies much lower than the blade vibration frequency of interest, they exploit the aliasing effect of the measurement setup to obtain the blade natural frequency.

Reinhardt et al. (1995) use least-squares curve fitting to approximate blade vibration amplitude and frequency at very low rotation speeds (80 to 100 RPM). Reinhardt and his co-workers excite the entire rotor assembly axially with an actuator using a sine wave of constant amplitude and frequency. As with Cookson and Bandyopadhyay (1980), the equations derived are not valid for impulse excitation. The proposed method is further limited to frequencies with more than two vibration cycles during the signal length, implying a lower frequency limit. To obtain lower frequency information, they propose a modal filtering method that will allow blade vibration measurement without rotation speed limitations. However in order to implement the proposed filtering technique, several points along the length of the blade need to be measured simultaneously.

### **1.5.9.2 Lagrangian Laser Doppler Vibrometry**

Lagrangian Laser Doppler Vibrometry entails using an LDV to take measurements in a moving reference frame (Castellini and Santolini, 1998:44). The two modes of implementing this measurement approach are known as TLDV and Continuous Scanning Laser Doppler Vibrometry (CSLDV).

#### **1.5.9.2.1 Tracking Laser Doppler Vibrometry**

Quite a number of literature resources are available on this subject. This approach to blade vibration measurement involves the synchronous movement of the laser beam with the rotor in order to follow a specific point on a specific blade.

There are two principal ways to implement TLDV. The first is purely mechanical as used by Sever (2004). Sever uses a conical mirror to direct the laser beam reflected from a 45° mirror installed on the shaft end, onto the rotating blade. The second implementation is to control the mirrors of a Scanning Laser Doppler Vibrometer

(SLDV) in such a way as to trace a circular pattern in synchronization with the shaft rotation speed, thereby following a specific point on the blade.

According to Halkon and Rothberg (2006:1295) tracking vibrometry significantly reduces speckle noise in the measurement of a rotating target. This technique does however introduce scan frequency components into the measured spectra. Misalignment between the axis of scanning system and that of the target rotation axis introduces a DC component as well as a  $1\times$  scanning frequency component, both of significant amplitudes. Furthermore, the dual mirror configuration of the SLDV introduces a  $2\times$  scanning frequency component, the amplitude of which is influenced by the mirror separation distance, the scanning radius as well as the standoff distance from the target. Although other integer multiple components of the scanning frequency are introduced as well the DC,  $1\times$  and  $2\times$  components are the most significant.

Lesne et al. (1985) use a tracking laser vibrometer to construct an inverse Campbell diagram of the blade tip vibration of a rotating blade.

Jacobs and Grady (1977) make use of servo scanning mirror as well as a parabolic mirror to perform TLDV circumferentially on an axial-flow machine.

### **1.5.9.2.2 Continuous Scanning Laser Doppler Vibrometry**

The term CSLDV refers to the application of an SLDV where the laser beam is moved continuously across a stationary test surface. Sriram et al. (1992:172) note that when using CSLDV, the measured velocity signal is modulated by the structure's Operational Deflection Shape (ODS). Scans can be performed at uniform or sinusoidal scanning rates. Stanbridge and Ewins (1999) demonstrate how modal testing can be accomplished at discrete excitation frequencies using CSLDV. When a uniform scan rate is used, the resulting LDV signal can be demodulated by multiplication of in-phase and quadrature signals at the excitation frequency. When sinusoidal scan rates are considered, the resulting LDV signal spectrum contains sidebands centred around the excitation frequency and spaced at harmonics of the scanning frequency. Fourier coefficients can then be obtained from these side bands. By repeating the scans for a range of discrete excitation frequencies, it is then possible to perform conventional modal analysis on these measurements.

Schwinshackl et al. (2010) concur, stating that the processing of signals acquired with CSLDV using sinusoidal scan rates occurs in the frequency domain whereas signal processing from uniform rate scanning occurs in the time domain. These authors also note that the uniform scanning rate approach can be used on structures with surface discontinuities whereas the sinusoidal scanning rate approach cannot.

### **1.5.10 Radar proximity sensors**

Chuckpaiwong (2003) presents a technique using phase-based continuous-wave radar that allows high speed, micro scale measurements with the sensor. Chuckpaiwong (2003:10-11) gives an outline of the capabilities of the radar sensor. The sensor's accuracy is comparable to that of eddy current sensors and has an operating range in the order of meters. The bandwidth and operating temperature range of the sensor exceed that of optical sensors and can be used in a contaminated environment as line-of-sight is not necessary. Chuckpaiwong furthermore states the price of the sensor to be comparable to that of normal eddy-current sensors.

Holst (2005) studies the use of the same sensor as a blade tip TOA measurement probe and focuses on geometric factors affecting the spatial filtering by the sensor. Holst notes that microwave reflection by the blade surroundings will influence the measurements.

## **1.6 Blade vibration measurement systems**

### **1.6.1 Available systems**

Von Flotow et al. (2000) review a number of techniques used for blade vibration monitoring. Faults that can be picked up with such measurements include thermal and centrifugal expansion, spool imbalance as well as crack growth damage. Following a patent search on the subject of blade health monitoring, the authors found over 60 such patents, half of which address clearance measurement and a third that are concerned with vibration using blade TOA. Von Flotow and his co-workers note that the worldwide market for these systems was less than \$5 million per year in 2000 and did not support product development at that time.

Von Flotow et al. (2000:439) summarize health monitoring and prognostic capabilities of blade vibration measurement systems. According to the authors it may be possible to anticipate HCF failure of blades. They note that resonance, amplitude and damping changes were under investigation (at the time of their publication) as

reliable damage indicators or “failure precursors”. Von Flotow and his co-authors furthermore state that development is required in order to have a fully autonomous system. According to them all laboratory systems (current to publishing) require much human intervention.

Drumm and Haase (2000) discuss the HiBand system of ExSell Instruments. This system can be used for the monitoring of several on-line parameters such as HCF blade vibration and LCF disk cracking of turbines. By using multiple element capacitive sensors (called MasterPlex sensors), they are able to measure high-bandwidth vibrations (20 MHz) at a high signal-to-noise ratio. Similar to torsional vibration measurements using shaft encoders, the system in effect digitizes the position of blades passing the sensors. The MasterPlex sensors can be made for permanent installations into rub strips and high temperature applications of over 2000 °F (1093 °C). Accurate installation of the MasterPlex sensors is very important for tip clearance measurements, but this should not have a substantial effect on blade vibration measurements. Very interestingly, Drumm and Haase (2000) note that disc cracks influence the centre of mass of the rotor. Also according to them, rotor cracks distort the disc strain fields, causing minute changes in the unbalance of the system. The authors note that light probes are not suitable for certain applications such as steam turbine blade vibration measurements. However, from Drumm and Haase's discussion, the ExSell Instruments HiBand system is very suitable for large steam turbine applications when use is made of MasterPlex sensors.

## **1.6.2 Shortcomings of available systems**

According to Beaumont (2004) and Hueck (2004) currently no on-line system is available for detecting blade cracks. Furthermore Hueck refers to a case where a 30% crack was present in a blade while the monitoring system (blade tip TOA) only detected a vibratory change of 0.1%. Hueck also states that the system in consideration, which is available from one of the top steam turbine manufacturers internationally, is limited to bandwidth of 100 Hz.

## **1.7 Experimental related issues**

### **1.7.1 Non-contact blade excitation techniques**

Due to the sensitivity of a bladed disc to mistuning (as discussed in Section 1.2.3.2), non-contact excitation of the structure is necessary for operational testing as well as modal analysis.

Mansidor (2002) uses eddy-current as well as air-jet excitation on the blades of a disc rotating in a vacuum. Although Mansidor measures the air pressure of the air-jets, no measurement or approximation is made of the force exerted on the blades by the air-jets.

Vanlanduit et al. (2007) do however make use of calibration curves to approximate the exerted forces by an impinging air-jet. Using an on-off control valve, the authors are able to perform modal analyses up to 1 kHz.

Truman et al. (1961) use a siren-type pulsed-air vibrator to excite stationary blades. The vibrator consists of a speed-controlled slotted disk rotating relatively to a stationary slotted disk, allowing the frequency control of resulting air pulses. The authors note that the subsequent vibrations in the stationary blade occur as a result of these pulsations. The amplitude of the blade vibration is determined by the airflow of the pulses. Truman and his co-workers state that airflow, nozzle-to-surface spacing and the air-jet angle-of-attack relative to the target surface are the main factors determining the dynamic behaviour of the forced blade.

Ziegler (1994) makes use of electromagnetic and air-jet excitation for shrouded and non-shrouded blades respectively.

With regards to stationary modal testing, impact hammer excitation is still more desirable in terms of accuracy since the applied force can be directly measured. Although not a non-contact excitation method in the strictest sense, structural modification due to additional mass is minimized.

## **1.8 Finite element modelling**

Gadala and Byrne (1986) discuss some issues with regards to finite element modelling of blades and present a comparative study for various 2-D and 3-D blade root models. The authors state that the incorporation of centrifugal stiffening is crucial for the dynamic analysis of blades as the blade natural frequencies may rise by up to 30% from their unstressed values as a result.

### **1.8.1 Model updating based on Frequency Response Functions**

The most promising technique of model updating is that of the FRF-based technique. This technique of model updating makes use of measured FRFs to directly update a finite element model.

According to Ewins (2000:462) this technique overcomes the need for large numbers of measurement points in order to capture high order mode shapes. This is due to the fact that FRF data contain information on in-range as well as out-of-range modes (Imregun and Visser, 1991) whereas modal data contain approximation information only on in-range modes.

Furthermore, response data represent the actual dynamic behaviour of the test structure more accurately than does the modal data extracted from these measurements due to the identification errors involved with the latter. These errors are caused by approximations and assumptions of modal property extraction. Imregun et al. (1995) list the fact that this technique does not require modal analysis as one of its main advantages.

In his software package, Balmès (1997:2-147) implements iterative FEM updating using the sum of the squared logarithmic differences between the measured and the numerical FRFs as the objective function.

## ***1.9 Issues with regards to Laser Doppler Vibrometry***

### **1.9.1 Speckle noise**

Martarelli and Ewins (2006) present an in-depth study into the analysis of speckle noise in the context of CSLDV along with a mathematical model for the effect of speckle noise. The two authors make a number of interesting remarks with regards to the nature of speckle noise. The first of these is that if the test structure is scanned repeatedly along the same line by the laser beam, the speckle patterns will have a constant spatial distribution. This also means that the noise effect will be concentrated in the frequency domain at the scan frequency and its harmonics. Martarelli and her co-author determined experimentally that as the scanning speed increases, the speckle noise in a measurement increases at the scanning frequency and its harmonics. Furthermore as the scanning speed increases, the broadband noise floor resulting from the speckle noise increases.

According to Martarelli and Ewins it is essential that in choosing a scanning frequency, its harmonics do not overlap with a natural frequency of the structure in order to derive a reliable response. When the scanning frequency is chosen accordingly, the authors state that the noise influence can be neglected by performing a targeted Fourier analysis at the scanning frequency and its harmonics.

Rothberg (2006) performs a study into the fundamental mechanisms of speckle noise occurrence in LDV measurements with specific application to out-of-plane vibration of rotating discs. Rothberg also presents a numerical simulation for the purpose of predicting speckle noise levels in a measurement. The author confirms the statement by Martarelli and Ewins (2006:2279) that although speckle noise affects the Doppler signal in terms of amplitude and phase modulation, it is the phase modulation effect that is of major concern.

Rothberg et al. (1989) identify three sources of speckle-noise namely target tilt as well as in-plane motion and rotating motion.

Denman et al. (1996) looks at the reduction of speckle noise in the measurement of vibration on a rotating structure by means of optimization of detector/target separation. The authors show numerically that speckle noise decreases with an increase in number of speckles in the speckle pattern incident on the detector. Since speckle size increases (and thus number of incident speckles decreases) along with detector/target separation due to light dispersion, it is desirable to have a small detector/target separation. However when the detector/target separation is very small, variance in the speckle pattern increases greatly. The aim is thus to find the optimum detector/target separation distance between these extremes. The authors show this experimentally and indirectly suggest the experimental determination of optimum detector/target separation.

### **1.9.1.1 The nature of speckle noise**

From the literature, the characteristics of speckle noise can be summarized as follows:

1. For a recurring speckle pattern change, the speckle noise will be of a pseudo-random nature. (Rothberg, 2006:4526; Martarelli and Ewins, 2006:2279; Halkon and Rothberg, 2006:1294; Rothberg et al., 1989:518). As a direct result of this, the speckle noise will repeat at the rotation frequency in the case of ELDV.

2. In the frequency domain, speckle noise manifest itself as approximate equal amplitudes at the pattern repeat frequency and its higher-order harmonics. (Rothberg, 2006:4526; Martarelli and Ewins, 2006:2279; Halkon and Rothberg, 2006:1294, Rothberg et al., 1989:518)
3. Speckle noise introduces low-level broadband noise to the measurements. (Rothberg, 2006:4525; Martarelli and Ewins, 2006:2279; Halkon and Rothberg, 2006:1294)
4. In the frequency domain, high orders of prevalent harmonics of the pattern repeat frequency and the sharpness of these peaks are classic characteristics of speckle noise. (Halkon and Rothberg, 2006:1294)
5. Denman et al. (1996) refer to speckle noise as “Doppler signal phase modulation” and “frequency broadening”

### 1.9.1.2 Noise cancellation

Wilmshurst and Halliwell (1993) present an article concerned with speckle-noise cancellation with excellent results. In their application, the authors use a rotating disc in the place of a Bragg cell to facilitate frequency shifting in a LDV for the purpose of determining the vibration direction of a test object. This rotating disc introduces speckle-noise in the reference signal, which Wilmshurst and Halliwell succeed in attenuating. In order to do this, the authors use a second rotating disc much like a shaft encoder for phase-locked loop correction of a measurement with excitation (speckle-noise and vibration information present) as referenced to a 256-sample time averaged measurement without excitation (speckle-noise dominant in signal). According to the authors, the number of time averages in the reference signal reduces the amplitude of random noise in the signal by a factor of the inverse of the square root of the number of averages.

Wilmshurst and Halliwell (1993) continue to describe the effect of number of time averages on the spectrum of the reference signal. As the number of time averages increases, the widths of harmonic peaks of the disc rotation frequency in the spectrum become narrower. Wilmshurst and his co-worker further use a periodic weighting signal proportional to the time derivative of the reference signal to extract useful information from the speckle-noise contaminated signal. The speckle-noise contaminated signal is multiplied by this weighting function and then integrated.

The two authors perform the noise cancellation in the time domain and go to quite an extent to compensate for inaccuracies caused mainly by speed fluctuations in the

rotating disc. However, these inaccuracies should be easy to overcome if the signal conditioning is performed in the angular domain.

Antoni and Randall (2004b) present a frequency domain noise cancellation algorithm. The minimum sequence length is determined by the inverse of the required frequency resolution and the time delay in the algorithm is given to be proportional to the reciprocal of the noise bandwidth (Antoni and Randall, 2004a).

### **1.9.2 Effect of geometry on measurements**

According to a number of papers (Kulczyk and Davis, 1973:1018; Halliwell, 1996:407; Halkon and Rothberg, 2006:1287), the geometry of a vibrating target does not directly influence CSLDV measurements. In an analysis by Bell and Rothberg (2000:247) this is proven analytically for ELDV implemented on a rotating shaft with an arbitrary cross section.

### **1.9.3 Practical issues**

Although Kadoya et al. (1995) focus on the blade tip TOA measurement application of laser probes, they do address a number of very important practical issues with regards to measurement with the probes in a steam turbine environment. To protect the probe from erosion and to maintain air-tightness, the authors use sapphire glass to seal the probe tip. In order to measure with the probe in the presence of water droplets, Kadoya and his co-authors use a 40 mW laser light source. The probe is arranged so that receiving fibres surround the transmitting quartz fibre. The authors also highlight the importance of perpendicularity between the laser beam and the blade surface to ensure sufficient reflectivity.

Aono et al. (1985) also present a paper on laser probes for TOA. They studied the effect of surface condition of compressor blades (in terms of dust and oil deposit) on the signal quality of the reflected light. Test results for a worst case scenario were favourable for TOA measurements.

## **1.10 Signal processing**

Considering the operational speeds of turbomachinery, it is quite clear that the measured ELDV vibration signals from individual blades will be very short. For a typical steam turbine operating at 50 Hz, the signal length of one measurement for an individual blade is about 0.5 ms. Traditional signal processing techniques such as

FFTs and nonparametric PSD estimations are limited in terms of frequency resolution (Lobos et al., 2006:219; Gamba and Shimamura, 2005:702), making them inappropriate for such short signals. For the sample length considered, a minimum frequency resolution of only 2 kHz is attainable with these techniques. This means that traditional signal processing techniques are not effective in this instance for damage detection.

Alternatively, parametric and subspace spectrum estimation techniques can be utilized (The Mathworks, 2006:3-7). As opposed to nonparametric estimation where the PSD is directly estimated from the signal, parametric methods estimate the PSD from a model of the signal using Autoregressive (AR) techniques. Giordano and Hsu (1985) note that these AR techniques make it possible to identify dominant spectral peaks masked in normal periodograms. Typical methods used are the Yule-Walker AR method and the Burg method and can yield higher resolutions for short signals as compared to nonparametric methods. According to Giordano and Hsu (1985) the maximum entropy method formulated by Burg is very well suited particularly for short signals. The Burg method is however prone to frequency splitting and is sensitive to the initial phase of the signal analyzed (Marple, 1987:225,227)

Subspace methods yield spectrum estimates based on eigendecomposition of the correlation matrix of the signal. Examples include the Multiple Signal Classification (MUSIC) method and the Eigenvector (EV) method.

According to Gamba and Shimamura (2005:702) and Fante (1988) however, these alternative methods yield superior results only at high SNRs. Fante (1988) states that at SNRs of lower than ten, ARMA modelling rather than AR modelling should be used to estimate the spectra. According to Marple (1987:231) this is due to the fact that the all-pole model assumed with AR techniques is no longer valid when noise is present.

Gamba and Shimamura (2005:702) propose the Iterative Noise Variance Estimation (INVE) technique based on low-order Yule-Walker equations to improve the results. From analytical results, the authors show this technique to be more noise-robust than the popular spectrum estimation techniques.

Hirata (2005) proposes the use of NHFA for short data records where the frequency resolutions obtainable with Harmonic Fourier Analysis (HFA) are too coarse to yield useful information. As in HFA, the time signal is also considered as the summation

of sine and cosine components. However, these components can be at arbitrary frequencies (i.e. not necessarily at integer multiples of the fundamental frequency). Steele (1999) employs a similar methodology to estimate components in ocean wave data.

Muraoka and Nishioka (2004) investigate the frequency limit of NHFA (which they refer to as generalized harmonic analysis) by considering a signal consisting of two sinusoids at different frequencies. From the conclusions based on their results, it is clear that the minimum resolvable frequency resolution between two sinusoidal waves is still determined to an extent by the  $1/t$  limitation as per classic Fourier analysis. The authors also note that the phases of the sinusoids influence the frequency resolution. According to Muraoka and his co-author, rectangular windowing of a signal is most suited for NHFA.

### **1.11 Scope of research**

The literature study covers a broad range of topics related to on-line turbomachinery blade condition monitoring. From this literature study, the scope of this research work is defined in the following paragraphs.

On-line blade vibration information contains crucial information for the on-line condition monitoring of these components. To perform these measurements, a number of options present themselves. The most intuitive approach is to install sensors such as strain gauges on the blades. However the limited life spans of such systems negate their long term use on industrial rotors. Measurements can also be obtained using TLDV or ESPI, with both of these approaches requiring blade line-of-sight over a significant rotor angle. This of course is not feasible for most industrial rotors due to the presence of rotor casings, guide vanes or other structural elements. Blade tip TOA monitoring systems are used in industry. Nevertheless the drawback of these systems is the large number of sensors required to obtain useful measurement bandwidths. An alternative approach is to measure blade vibrations in an Eulerian fashion. This measurement approach requires a non-contact sensor with a high bandwidth and a long stand-off distance. Radar proximity sensors are promising sensors for this application although effects such as spatial filtering, blade geometry and microwave reflection by surroundings need to be taken into account.

Measurements acquired by means of ELDV however are not affected by these factors. LDVs are capable of measuring large dynamic ranges from extremely small vibrations to large vibrations up to 30 m/s. These instruments furthermore have measurement bandwidths from 0 Hz up to several MHz. In an industrial environment the laser beam transmission can be accomplished with fibre optics, thus removing the sensor itself from the operating environment. For these reasons, ELDV is the main measurement approach in this thesis using the Polytec PSV300 SLDV at the University of Pretoria.

The two main challenges faced with ELDV as applied to rotating blades, are sufficient laser reflectivity from the blades, as well as the brief nature of the measured vibration signals. The challenge with regards to laser reflectivity could be overcome by either surface treatment of the blades or by increasing the strength of the laser source. Since the latter option is not available on the Polytec PSV300, blade surface treatment is performed in the form of reflective material installed on the test rotor.

The ELDV measurement technique is studied analytically on a vibrating cantilever beam translating longitudinally at constant speeds and the results are verified experimentally. From this study, a numerical simulation approach of ELDV is proposed and evaluated using standard simulation techniques. This approach is then extended to rotating blades.

A simple single stage axial-flow test rotor is used for experimental testing at relative slow rotation speeds up to a maximum of 1500 RPM. The blades are straight and flat and are attached to the rotor hub by means of clamping to ensure repeatable boundary conditions at the blade roots. A single stationary air-jet is used to simulate guide vane excitation of the rotating blades and is controlled to yield repeatable excitation. The test rotor (installed with a high resolution shaft encoder) is driven by speed-controlled motor and various pre-sets are used to ensure repeatable rotor speed settings.

The experimental simulation of cracks is not a trivial exercise. This thesis is however more concerned with the effect of damage on blade vibration than the damage mechanisms themselves. For this reason, damage is simulated in the test rotor by means of slot cuts into the blade leading edges close to the blade roots using a high-speed rotary tool. This option is attractive since it can be performed *in situ*, thus eliminating blade root boundary condition changes due to removal and reinstallation of the blades during the testing phase.

Prior to dynamic testing, stationary modal testing is conducted on the test rotor and blades. A modal hammer is used for excitation and the responses are measured via LDV. The choice of excitation and measurement are to minimize any modification of structural dynamics by additional sensor mass and so ensure accurate FRF measurements.

Initial testing is carried out with a single blade on the rotor to simplify signal processing by eliminating the effects of global modes due to the presence of other blades. Measurements are recorded at a fixed rotor speed and for increasing damage on the blade. The signal processing methodology developed from these measurements is then applied to measurements from a fully bladed rotor with various damage levels on multiple blades. Four different rotor speeds are considered.

The brief nature of ELDV blade vibration signals presents the main challenge of this thesis in terms of signal processing. Various standard and non-standard signal processing techniques are investigated to obtain blade health indicators. NHFA in

particular is well suited to extract information from these short signals and a study of the analysis technique is conducted, showing that care must be taken when performing NHFA due to frequency component cross-talk. A sensitivity analysis shows that this phenomenon can be exploited for frequency shift detection.

NHFA is performed on the single-blade measurements over bands around various reference frequencies. The Maximum Absolute Unwrapped Phase Angle Trends (MAUPATs) over these bands are shown to be robust indicators of blade health deterioration. MAUPATs are calculated on the multi-blade measurements and the progressive standard deviations of the individual blade MAUPATs are demonstrated as useful for distinguishing between healthy and damaged blades. Evaluating also cross-correlation coefficient and RMS value trends of these measurements, an ANN is successfully trained to quantify the conditions of the individual blades.

FEMs of the different test rotor configurations are constructed and updating thereof is performed using FRF-based model updating. To incorporate the proposed numerical simulation approach of ELDV, the FEM mesh nodal resolutions are specified accordingly along the measurement curves. Damage is simulated in the FEMs to represent the experimental damage and centrifugal stiffening is included in simulations while gyroscopic effects are discarded. The FEMs are used to verify experimental results.

## **1.12 Document layout**

Chapter 1 contains a thorough literature study covering a broad range of topics related to on-line turbomachinery blade condition monitoring. In this chapter, the research scope is also defined.

In Chapter 2, an analytical study of ELDV is conducted on an Euler-Bernoulli cantilever beam that translates at a constant velocity relative to a stationary LDV. A numerical simulation approach of ELDV is then proposed using a Lagrangian Vibration Response Matrix (LVRM) for a reference scanning speed. The feasibility of using interpolation on this LVRM to estimate responses for other translation velocities is also investigated. This simulation approach is extended to axial-flow rotating blades and the findings of the analytical ELDV study are verified experimentally.

Chapter 3 investigates the feasibility of using ELDV as an on-line blade vibration measurement technique a single-blade experimental rotor. ELDV and TLDV measurements are presented for increasing damage levels on the blade and vibratory phase angle shift is illustrated to be a valuable blade health indicator. NHFA is utilized to obtain phase angle information from the ELDV measurements and MAUPATs over bands around reference frequencies are established as robust blade health indicators. After FEM validation, the experimental results are verified with the aid of FEM simulations.

ELDV measurements on a multi-blade test rotor are considered in Chapter 4 with the tests conducted at different rotor speeds and increasing damage levels on various blades.

Considering the progressive standard deviations of MAUPATs as well as some time domain parameters, it is proven that individual blade conditions can be quantified via ANN implementation. Individual blade natural frequencies are also accurately approximated from ELDV rundown signatures.

Chapter 5 concludes the work in this thesis and additional work for future research is proposed.

### **1.13 Publications**

This work forms part of a research initiative consisting of two parts. The first part is contained within the master's dissertation of the author and was concerned with the development of an on-line fan blade damage detection methodology using piezoelectric strain sensors and accelerometers installed on the blades of a four-blade test rotor. Using ANNs it was shown experimentally that on-line blade condition monitoring can be performed using less than one sensor per blade. ANNs were also trained on FEM results and successfully applied to experimental measurements. The outputs from the author's master's work are as follows:

1. Oberholster, A.J. (2004). *The development of an on-line fan blade damage detection methodology*. Master's dissertation. Pretoria: University of Pretoria.
2. Heyns, P.S., Oberholster, A.J. (2004). *On-line fan blade damage detection*. Proceedings of the 11<sup>th</sup> International Congress on Sound and Vibration: St. Petersburg, Russia, 2921-2928.
3. Oberholster, A.J., Heyns, P.S. (2006). On-line fan blade damage detection using neural networks. *Mechanical Systems and Signal Processing*, 20(1), 78-93. (DOI 10.1016/j.ymsp.2004.09.007).

4. Heyns, P.S., Stander, C.J., Oberholster, A.J., Schön, P.P., Ngwangwa, H.M. (2007). *Machine and structural health monitoring: Some recent developments*. Proceedings of the 3<sup>rd</sup> International Conference on Structural Engineering, Mechanics and Computation: Cape Town, South Africa, 124-129.

This thesis contains the second part of the research initiative and focuses on using a non-contact measurement approach. The following conference papers and articles were produced during the course of this thesis:

1. Oberholster, A.J., Heyns, P.S. (2007). *The application of Eulerian laser Doppler vibrometry to on-line damage detection of axial-flow turbomachinery blades*. Proceedings of the 20<sup>th</sup> International Congress on Condition Monitoring and Diagnostic Engineering Management: Faro, Portugal, 637-645.
2. Oberholster, A.J., Heyns, P.S. (2008). *A study of the non-harmonic Fourier analysis technique*. Proceedings of the 21<sup>st</sup> International Congress on Condition Monitoring and Diagnostic Engineering Management: Prague, Czech Republic, 361-370.
3. Oberholster, A.J., Heyns, P.S. (2009). Online condition monitoring of axial-flow turbomachinery blades using rotor-axial Eulerian laser Doppler vibrometry. *Mechanical Systems and Signal Processing*, 23(5), 1634-1643. (DOI 10.1016/j.ymsp.2009.01.001).
4. Oberholster, A.J., Heyns, P.S. (In press). Eulerian laser Doppler vibrometry: Online blade damage identification on a multi-blade test rotor. *Mechanical Systems and Signal Processing*. (DOI 10.1016/j.ymsp.2010.03.007).
5. Oberholster, A.J., Heyns, P.S. (In progress). On the measurement of circumferential vibration on rotating blades using laser Doppler vibrometry. *Experimental Techniques*.

## **Chapter 2 Eulerian Laser Doppler Vibrometry**

### **2.1 Introduction**

This chapter studies the ELDV measurement technique as applied to translating targets. To demonstrate the most salient characteristics of ELDV, an analytical study is conducted on a translating Euler-Bernoulli cantilever beam and ELDV is defined accordingly. The analytical ELDV equations are then expressed in numerical form and an approach for the simulation of ELDV is proposed. The effects of translation speed on ELDV measurements are studied as well and the feasibility of using the measurement technique as a condition monitoring tool is determined. The numerical and analytical results are confirmed experimentally after which the interpolation approach is extended to rotating axial-flow blades.

### **2.2 Analytical and numerical study**

#### **2.2.1 Cantilever beam theory**

It is useful for understanding the characteristics of ELDV to consider a cantilever beam of length  $l$ , vibrating under the influence of an arbitrary concentrated load  $F$ , while translating at a constant speed  $c$ , perpendicular to a stationary LDV (see Figure 2). This is in effect an application of CSLDV with a uniform scanning rate. Torsional, sideways and axial vibrations are not taken into account for this demonstration.

By considering the Lagrangian (i.e. the moving reference frame) vibration of the beam as a function  $t$ , the Lagrangian vibration displacement  $w_L$  can be obtained at an arbitrary discrete Lagrangian measurement position  $x_L$  using the well-known Euler-Bernoulli formulation:

$$w_L(x_L, t) = \sum_{j=1}^{\infty} W_j(x_L) \cdot q_j(t)$$

**Equation 4**

where  $W_j$  and  $q_j$  respectively are the characteristic function and generalized coordinate for the  $j^{\text{th}}$  mode of the cantilever beam with corresponding natural frequency  $\omega_j$  (Rao, 1995).

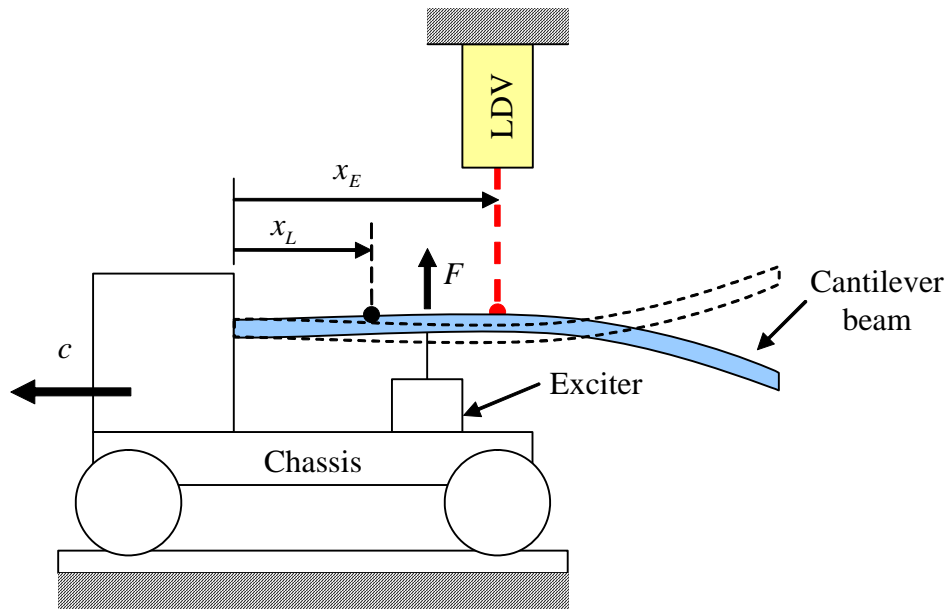


**Figure 2: Longitudinally translating cantilever beam**

Since LDVs measure vibration velocity it is desirable to find the Lagrangian vibration velocity  $v_L$  which obtained by appropriate differentiation of Equation 4:

$$v_L(x_L, t) = \frac{\partial w_L(x_L, t)}{\partial t} = \sum_{j=1}^{\infty} W_j(x_L) \cdot \frac{dq_j(t)}{dt}$$

**Equation 5**

### 2.2.2 ELDV analytical formulation

If the beam vibration is considered in the Eulerian (i.e. the stationary) reference frame, the Eulerian measurement position  $x_E$  is a function of  $c$  and  $t$  (i.e.  $x_E = ct$ ) and consequently does  $W_j$  become time dependent:

$$W_j(x_E) = W_j(ct)$$

**Equation 6**

Since both  $W_j$  and  $q_j$  are now functions of  $t$ , the contribution of the  $j^{\text{th}}$  mode to the observed vibration response is effectively the result of amplitude modulation of  $q_j$  by  $W_j$ . The Eulerian vibration velocity  $v_E$  is thus expressed by extending Equation 5 to the Eulerian reference frame:

$$v_E(c, t) = \sum_{j=1}^{\infty} W_j(ct) \frac{d}{dt} q_j(t) \text{ for } 0 \leq t \leq \frac{l}{c}$$

**Equation 7**

Since the setup in Figure 2 is effectively CSLDV with a uniform scanning rate, the amplitude modulation observation from Equation 7 is confirmed by Schwingshackl et al. (2010) who state that the ODS modulates the excitation signal.

### 2.2.3 Numerical simulation of ELDV

The main difference between Equation 5 and Equation 7 is the way in which the measurement positions are defined. Since  $c$  is assumed to be constant, it is possible to obtain  $v_E$  for discrete time instants  $t_n$  and discrete measurement positions  $x_{E,n}$  by simply considering the values of discrete  $v_L$ s at the corresponding times and measurement positions (i.e.  $x_{L,n} = x_{E,n}$ ). It is therefore possible to define an Eulerian Vibration Response (EVR) vector as:

$$\begin{aligned} \bar{v}_E &= [v_E(c, t_0), v_E(c, t_1), \dots, v_E(c, t_{N-1}), v_E(c, t_N)] \\ &= [v_L(x_{L,0}, t_0), v_L(x_{L,1}, t_1), \dots, v_L(x_{L,N-1}, t_{N-1}), v_L(x_{L,N}, t_N)] \end{aligned}$$

**Equation 8**

for  $x_{L,n} = x_{E,n} = ct_n$  with  $n = 0, 1, \dots, N$  and where  $N$  is the number of samples.

Equation 8 implies that it is necessary to have a Lagrangian Vibration Velocity Response (LVVR) vector  $\bar{v}_{L,n}$  available for each  $x_{L,n} = x_{E,n}$  over the entire measurement period:

$$\bar{v}_{L,n} = [v_L(x_{L,n}, t_0), v_L(x_{L,n}, t_1), \dots, v_L(x_{L,n}, t_N)]$$

**Equation 9**

If a fixed sampling frequency is used with a corresponding time interval  $\Delta t = t_n - t_{n-1}$ , and sampling is performed over the total length of the cantilever beam from root to tip,  $N$  is determined by the time required for the laser to traverse the full length of the cantilever beam (i.e.  $l/c$ ) divided by  $\Delta t$ . Since  $N$  must be an integer, the floor function is applied (rounded towards minus infinity):

$$N = \left\lfloor \frac{l}{c \cdot \Delta t} \right\rfloor$$

**Equation 10**

Equation 8 and Equation 10 have a number of implications since  $x_{L,n} = x_{E,n} = ct_n$ . Firstly, a new EVR has to be calculated for every different value of  $c$ . Secondly, if a FEM is used to calculate  $\bar{v}_E$ ,  $\bar{v}_{L,n}$  has to be extracted for each of the element nodes with locations corresponding to  $x_{E,n}$ . This implies that a different mesh density is required for every value of  $c$ .

This requirement can however be alleviated by utilizing an appropriate interpolation scheme on a Lagrangian Vibration Response Matrix (LVRM). This LVRM ( $\hat{V}_{L,c_{ref}}$ ) consists of row vectors with each row the  $\bar{v}_{L,n}$  for  $x_{L,n}$  corresponding to an arbitrary reference speed  $c_{ref}$ :

$$\hat{V}_{L,c_{ref}} = \begin{bmatrix} \bar{v}_{L,0} \\ \bar{v}_{L,1} \\ \vdots \\ \bar{v}_{L,N_{ref}} \end{bmatrix} = \begin{bmatrix} v_L(x_{L,0}, t_0) & v_L(x_{L,0}, t_1) & \cdots & v_L(x_{L,0}, t_{N_{ref}}) \\ v_L(x_{L,1}, t_0) & v_L(x_{L,1}, t_1) & \cdots & v_L(x_{L,1}, t_{N_{ref}}) \\ \vdots & \vdots & \ddots & \vdots \\ v_L(x_{L,N_{ref}}, t_0) & v_L(x_{L,N_{ref}}, t_1) & \cdots & v_L(x_{L,N_{ref}}, t_{N_{ref}}) \end{bmatrix}$$

**Equation 11**

with  $x_{L,n} = c_{ref}t_n$  and the reference sample length  $N_{ref} = \lfloor l/(c_{ref} \cdot \Delta t) \rfloor$ .

If a speed ratio  $k$  is defined as the ratio of the desired  $c$  to  $c_{ref}$ , i.e.  $k = c/c_{ref}$  and if  $k = 1$  (i.e.  $c = c_{ref}$ ), the Eulerian measurement positions  $x_{E,n}$  are identical to  $x_{L,n}$ . Thus Equation 8 holds for  $k = 1$  and can be expressed in terms of the LVRM:

$$\bar{v}_{E,c_{ref}} = \left[ \hat{V}_{L,c_{ref}}^{0,0}, \hat{V}_{L,c_{ref}}^{1,1}, \dots, \hat{V}_{L,c_{ref}}^{N_{ref}-1, N_{ref}-1}, \hat{V}_{L,c_{ref}}^{N_{ref}, N_{ref}} \right]$$

$$\therefore \bar{v}_{E,c_{ref}}^n = \hat{V}_{L,c_{ref}}^{n,n} \quad \text{for all } n = 0, 1, \dots, N_{ref}$$

**Equation 12**

where the superscripts indicate element numbers. In other words if  $k = 1$ , the EVR is obtained directly from the diagonal of the LVRM.

Similarly for other integer values of  $k$ :

$$\bar{v}_{E,k \cdot c_{ref}} = \left[ \hat{V}_{L,c_{ref}}^{k \cdot 0, 0}, \hat{V}_{L,c_{ref}}^{k \cdot 1, 1}, \dots, \hat{V}_{L,c_{ref}}^{k \cdot (N_k - 1), N_k - 1}, \hat{V}_{L,c_{ref}}^{k \cdot N_k, N_k} \right]$$

$$\therefore \bar{v}_{E,k \cdot c_{ref}}^n = \hat{V}_{L,c_{ref}}^{kn, n} \quad \text{for all } n = 0, 1, \dots, N_k$$

**Equation 13**

with  $x_{E,n} = x_{L,kn}$  and  $N_k = \lfloor N_{ref}/k \rfloor$  compensating for the reduction in number of samples from  $\hat{V}_{L,c_{ref}}$  to  $\bar{v}_{E,k \cdot c_{ref}}$ .

Equation 12 and Equation 13 are represented graphically by Figure 3 for different integer values for  $k$ . The LVRM and the various EVRs are shown for a vibrating cantilever beam (Table 1) excited with a 0.5 ms half-sine pulse.

When  $k$  is a not an integer it is necessary to perform interpolation. Satisfactory interpolation requires a careful choice of both  $\Delta t$  and position intervals  $\Delta x$  in  $\hat{V}_{L,ref}$ .  $\Delta t$  should be small enough to capture the vibration response at each position properly, whereas  $\Delta x$  should be small enough to capture the spatial variation in the vibration responses adequately.

**Table 1: Cantilever beam properties**

Young's modulus	223 GPa
Density	7770 kg/m <sup>3</sup>
Length	112.5 mm
Width	25 mm
Thickness	2 mm
Excitation force location from beam root	35.25 mm

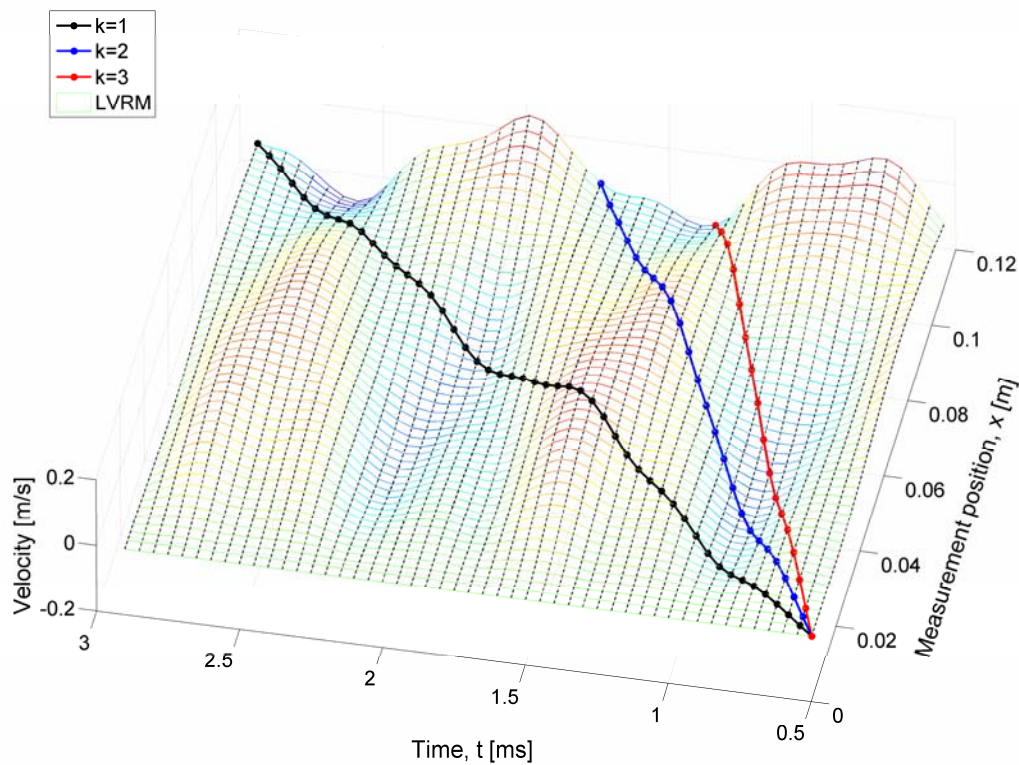


**Figure 3: LVRM and EVRs for integer values of  $k$**

To evaluate the accuracy of obtaining  $\bar{v}_E$  from  $\hat{V}_{L,c_{ref}}$  via interpolation for non-integer values of  $k$ , simulations were done in Matlab for a cantilever beam with the same properties as listed in Table 1, again excited with a 0.5 ms half-sine pulse. The time interval was fixed for a sampling frequency of 12 kHz, allowing the accurate simulation of the beam's first four natural frequencies.

An arbitrary  $c$  of 13.798 m/s was chosen to obtain the interpolated EVRs. Different LVRMs were calculated for integer values of  $c_{ref}$  ranging from 1 m/s to 20 m/s, so effectively varying  $k$ . The interpolated  $\bar{v}_E$ s were obtained from each of these LVRMs and compared with an  $\bar{v}_E$  for  $k=1$  (i.e.  $c_{ref} = 13.798$  m/s) to evaluate the accuracies of the interpolations. Linear and cubic spline interpolation methods were evaluated to determine the most suitable approach.

Figure 4 shows how the value of  $k$  affects the mean absolute error between the interpolated  $\bar{v}_E$ s ( $k \neq 1$ ) and the direct  $\bar{v}_E$  ( $k = 1$ ). Clearly it is beneficial to have a low value for  $c_{ref}$  (i.e. high  $k$ ) for  $\hat{V}_{L,c_{ref}}$ . It can also be observed that the cubic spline interpolation scheme provides results which are several orders of magnitude better than those obtained from linear interpolation.

Schwingshackl et al. (2010) also use interpolation in simulating uniform scan rate CSLDV measurements on a cylindrical FEM. In accordance with the observed advances of having a high  $k$  value, the authors use a high mesh density to obtain a LVRM. They do however not state which interpolation scheme they employ.

## 2.2.4 Effect of scanning speed

Since ELDV measurements are dependent on scanning speed, it is necessary to determine the extent of this influence. In this section the cantilever beam considered in Section 2.2.3 is subjected to a half-wave sine pulse of amplitude 10 N with duration of 0.5 ms. This choice of excitation was made to simulate an impulse force, allowing the simultaneous excitation of all the natural frequencies considered. The pulse duration was chosen to have an excitation bandwidth that encompassed the relevant natural frequencies. A sampling frequency of 12.8 kHz allowed sufficient measurement bandwidth to detect the beam's fourth natural frequency in the frequency spectra. In this section, the scanning direction will be from beam tip to root starting from  $t = 0$  s. When the initial displacements and velocities of the beam are set to zero, spectra can be calculated from the EVRs without having to use windowing

functions. This is an advantage as windowing functions may introduce distortions in the spectra.

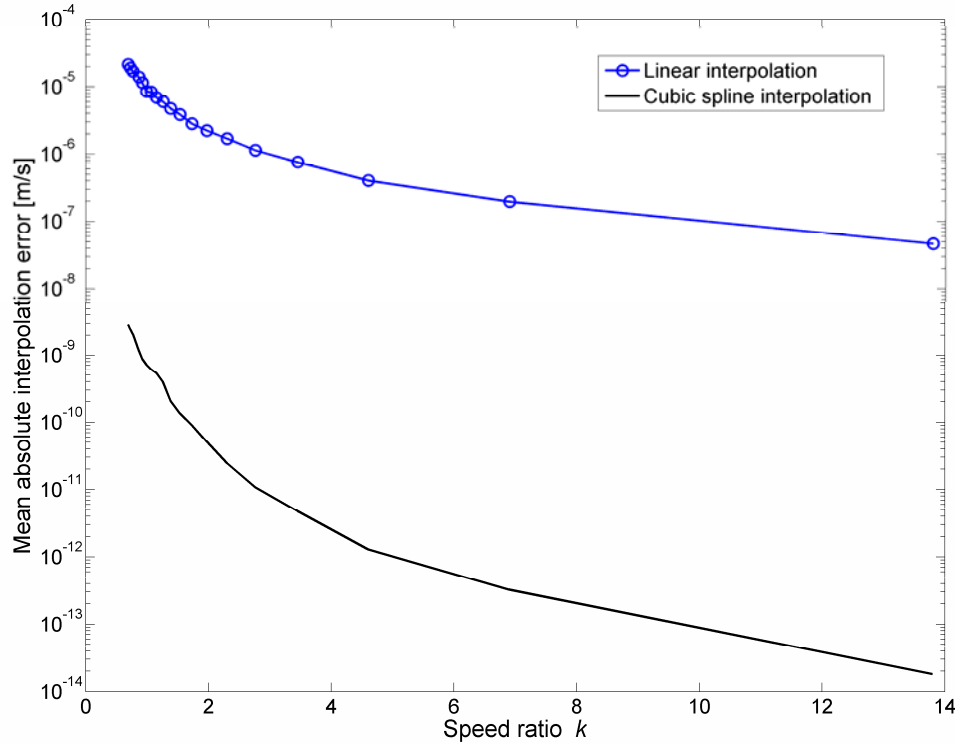


**Figure 4: LVRM interpolation scheme evaluation**

The  $\omega_j$ s of the cantilever beam were calculated analytically and are listed in Table 2:

**Table 2: Euler-Bernoulli cantilever beam natural frequencies**

$j$	$\omega_j$ [Hz]
1	136.8
2	857.0
3	2339.7
4	4702.5

### 2.2.4.1 Modulation frequency

Consider the PSD of the  $\bar{v}_E$  for  $c = 0.1125$  m/s (i.e. the sample length is 1 s) as depicted in Figure 5 with the red lines indicating the beam's  $\omega_j$ s. When a closer look is taken at the peaks, clear sidebands are visible around  $\omega_2$ ,  $\omega_3$  and  $\omega_4$ . Figure 6

shows this for  $\omega_4$  and verifies the observation of Section 2.2.2 with regards to amplitude modulation of  $q_j$  by  $W_j$  (Equation 7).

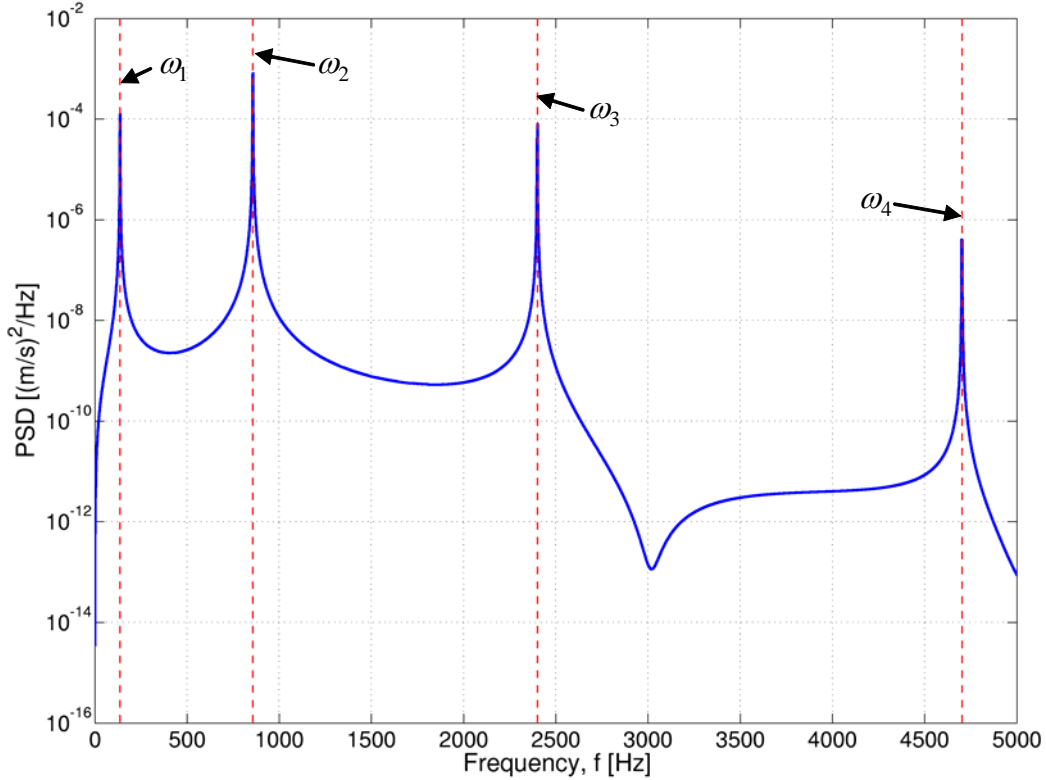


**Figure 5: PSD of  $\bar{v}_E$  for  $c = 0.1125$  m/s**

Since  $W_j$  is a function of  $c$ , its modulation frequency  $\Omega_j$  should be affected by  $c$  as well and the sideband separation in the spectrum should thus be proportional to  $c$ . To verify this, EVRs were calculated for different values of  $c$ . To increase the frequency resolution of the EVR spectra, each EVR was padded with zeros to yield a 0.1 Hz spectral resolution. The PSDs are shown in Figure 7 from which it is clear that  $\Omega_j$  increases with  $c$ . From this figure, the negative effects of zero padding are evident by the manifestation of decrease in peak amplitudes, increase in peak damping as well as the introduction of fundamental frequency harmonics. These effects were not of concern since only the frequencies of the modulation peaks were considered here.

To analytically determine the relationship between  $\Omega_j$  and  $c$ , it is necessary to study the definition of  $W_j$  as given by Rao (1995). In the context of ELDV,  $W_j$  is expressed as:

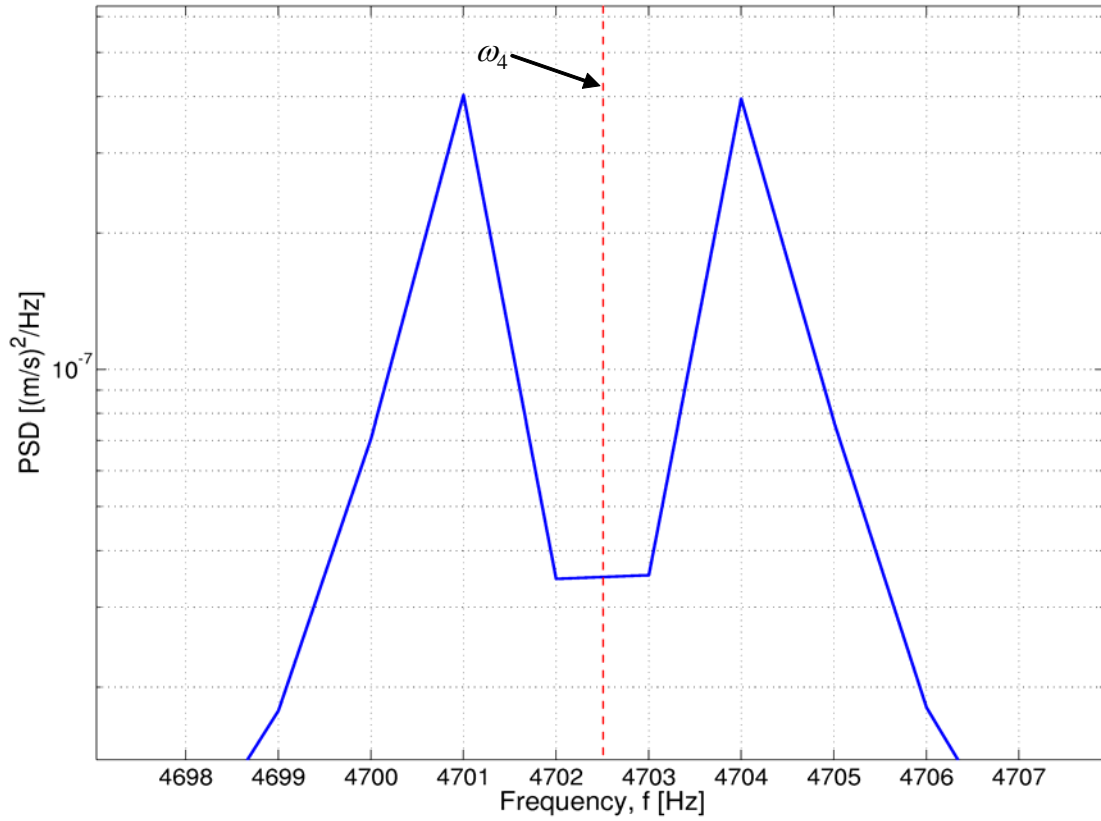


Figure 6: Sidebands around 4th natural frequency

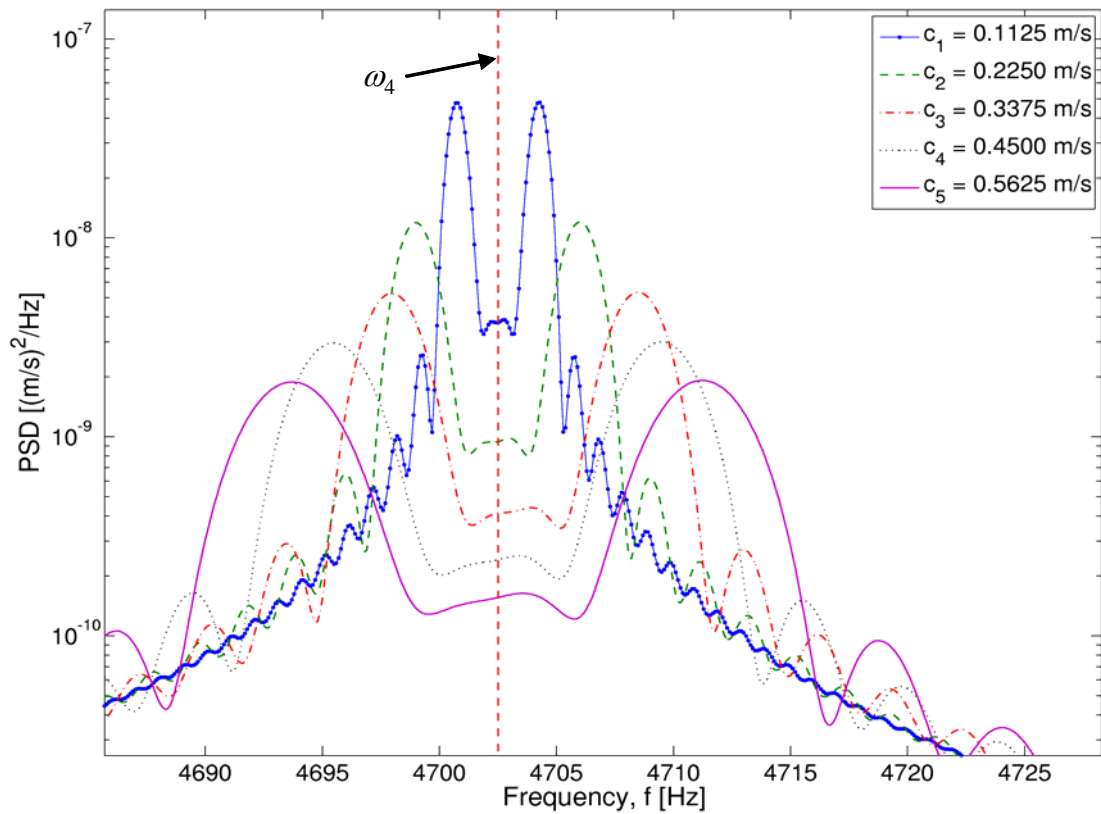
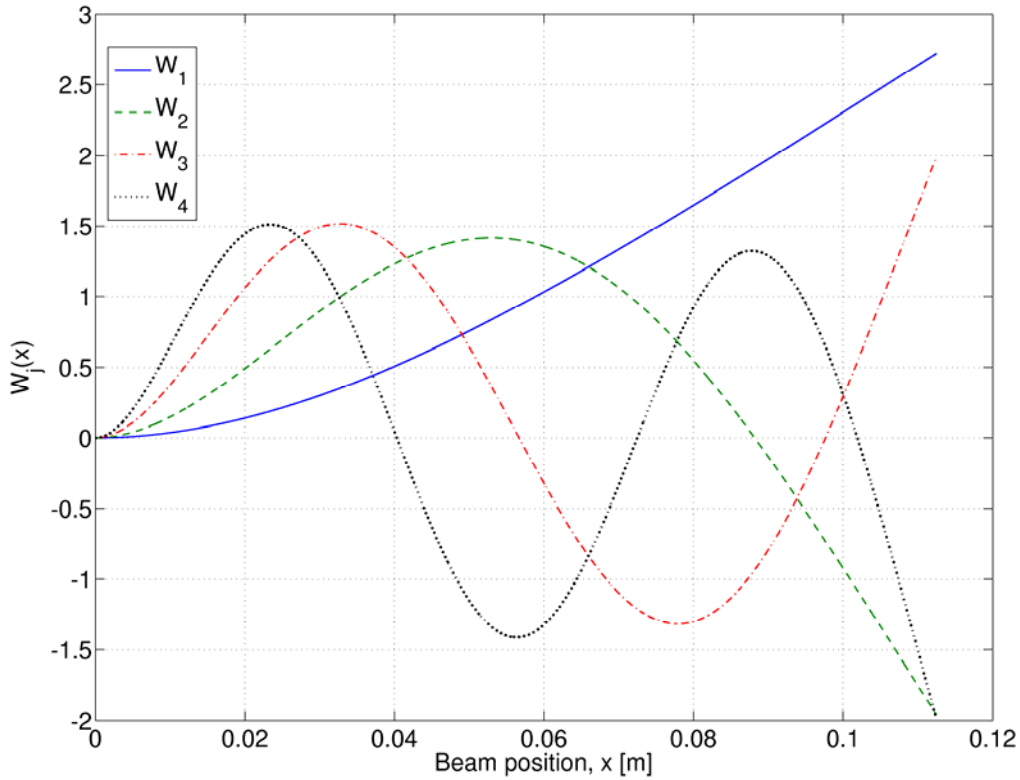


Figure 7: Effect of scanning speed on modulation sidebands separation

$$W_j(ct) = E_j \left[ \sin \beta_j ct - \sinh \beta_j ct - \left( \frac{\sin \beta_j l + \sinh \beta_j l}{\cos \beta_j l + \cosh \beta_j l} \right) (\cos \beta_j ct - \cosh \beta_j ct) \right]$$

**Equation 14**

with  $\cos \beta_j l \cdot \cosh \beta_j l = -1$ . The first four  $W_j$ s of the considered cantilever beam are shown in Figure 8.



**Figure 8: Characteristic functions  $W_j$**

Since  $E_j$  and  $(\sin \beta_j l + \sinh \beta_j l) / (\cos \beta_j l + \cosh \beta_j l)$  are constants and both  $(\sinh \beta_j ct)$  and  $(\cosh \beta_j ct)$  are not periodic functions (i.e. non-oscillating),  $\Omega_j$  is thus mainly dependent on the  $(\sin \beta_j ct)$  and  $(\cos \beta_j ct)$  terms.

$\Omega_j$  can thus be approximated in Hz as

$$\Omega_j(c) \approx \frac{\beta_j c}{2\pi}$$

**Equation 15**

Figure 9 compares the predicted values of  $\Omega_j$  from Equation 15 with the values obtained from the  $\bar{v}_E$  PSDs for different values of  $c$ . From Figure 9 excellent

correlation exist between the predicted and actual values of  $\Omega_j$  for  $j=2,3,4$ . However Equation 15 is clearly not valid for  $j=1$ . When referring to Figure 8 it is clear that  $W_1$  never crosses zero. Thus strictly speaking,  $W_1$  does not amplitude modulate  $q_1$  but rather amplifies  $q_1$  in an increasing fashion. For this reason  $\Omega_1 = 0$ , as verified by the spectral results of Figure 9.

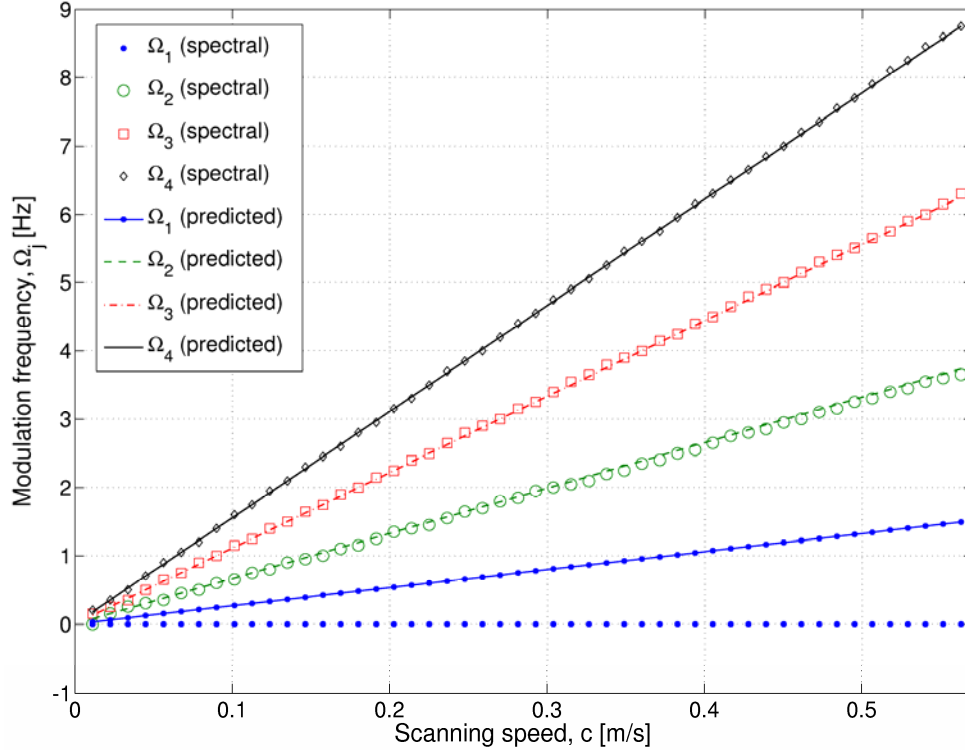


Figure 9: Comparison of actual and predicted values of  $\Omega_j$  for various values of  $c$

### 2.2.4.2 Frequency resolution

In order to accurately measure the vibration at a certain frequency, at least one complete vibration cycle at that frequency needs to be sampled at a sufficient sampling frequency. This has an important implication for EVR spectra, specifically with regards to the scanning speed.

The time it will take to perform a constant speed scan of the beam, is given as  $t_N = l/c$  and subsequently the frequency resolution is:

$$\Delta f = \frac{1}{t_N} = \frac{c}{l}$$

Equation 16

Equation 16 can be rearranged to find the maximum scan speed  $c_{\max}$  for which the minimum required frequency resolution  $\Delta f_{\min}$  can be obtained.

$$c_{\max} = l \cdot \Delta f_{\min}$$

**Equation 17**

Consider  $\omega_1 = 136.8$  Hz of the cantilever beam. The maximum scanning speed for which this frequency can be accurately detected is given by Equation 17 as  $c_{\max} = 15.39$  m/s. Figure 10 shows the FFTs for five different scanning speeds expressed as fractions of this  $c_{\max}$ . It can be shown that  $\omega_1$  is detected within 1 % for scanning speeds lower than  $0.17 c_{\max}$  and that at  $c_{\max}$ , the detected peak frequency has a 36% error. Thus although signal activity can be detected using a  $c_{\max}$  value as defined by Equation 17, to accurately obtain peak frequency from ELDV measurements requires the value of  $c_{\max}$  to be further reduced by a factor of 10:

$$c_{\max} = \frac{l \cdot \Delta f_{\min}}{10}$$

**Equation 18**

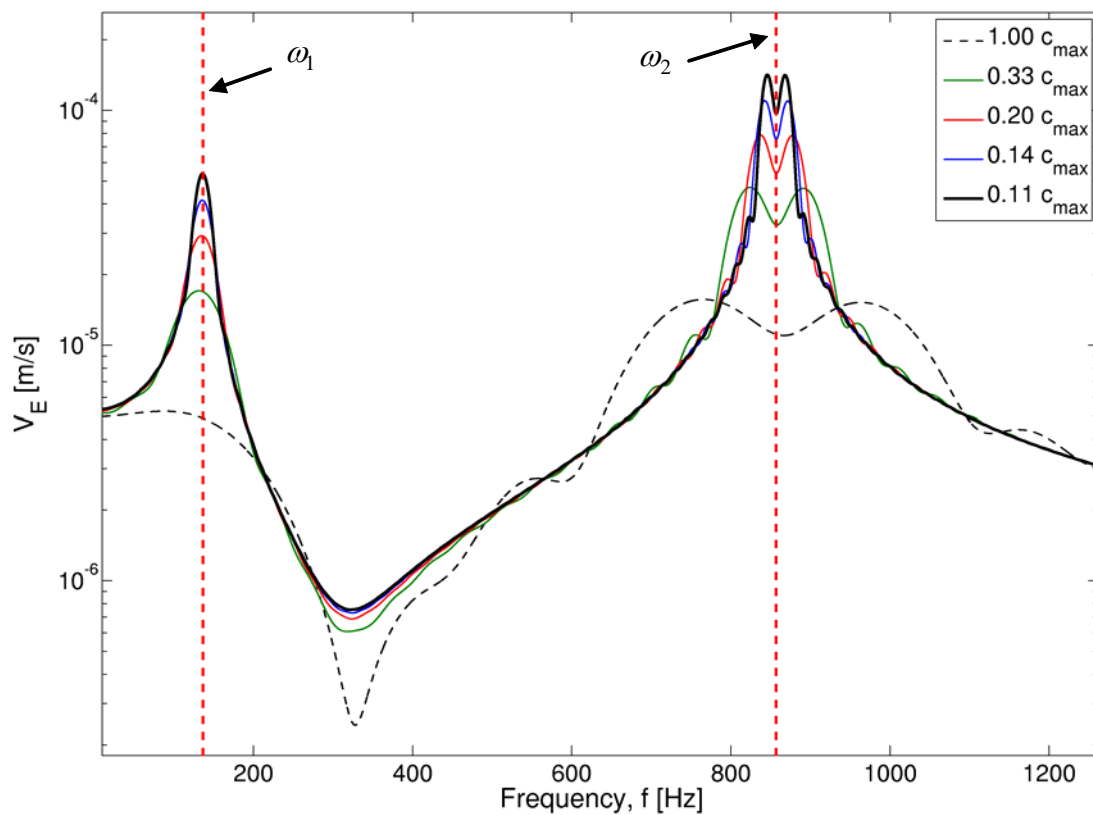


**Figure 10: Observed vibration FFTs for different scanning speeds**

### 2.2.5 Condition monitoring feasibility study

One of the main premises of condition monitoring using vibration signals is that damage as in the form of cracks reduces the stiffness of the structure, thereby leading to a decrease in structural natural frequencies. Although it would be desirable to simulate this type of damage in the FEM, it is computationally very expensive to obtain  $\hat{V}_{L,c_{ref}}$  with  $c_{ref}$  low enough to obtain a good spectral frequency resolution for the purpose of accurate peak shift detection.

To simulate crack-type damage in an Euler-Bernoulli beam on the other hand, is no small task, although it is definitely possible. However, since a decrease in natural frequencies is associated with a decrease in stiffness, natural frequency shifts can be induced in an Euler-Bernoulli beam by simply varying Young's modulus of the beam.

This was done for the beam of Section 2.2.3 with the Young's modulus decreasing from 223 GPa to 211.85 GPa (i.e. a 5% reduction). Figure 11 shows the results of these simulations in terms of the EVR PSDs in the vicinity of  $\omega_3$  for  $c = 0.1125$  m/s. The various EVRs were again padded with zeros to obtain a sufficient frequency resolution.

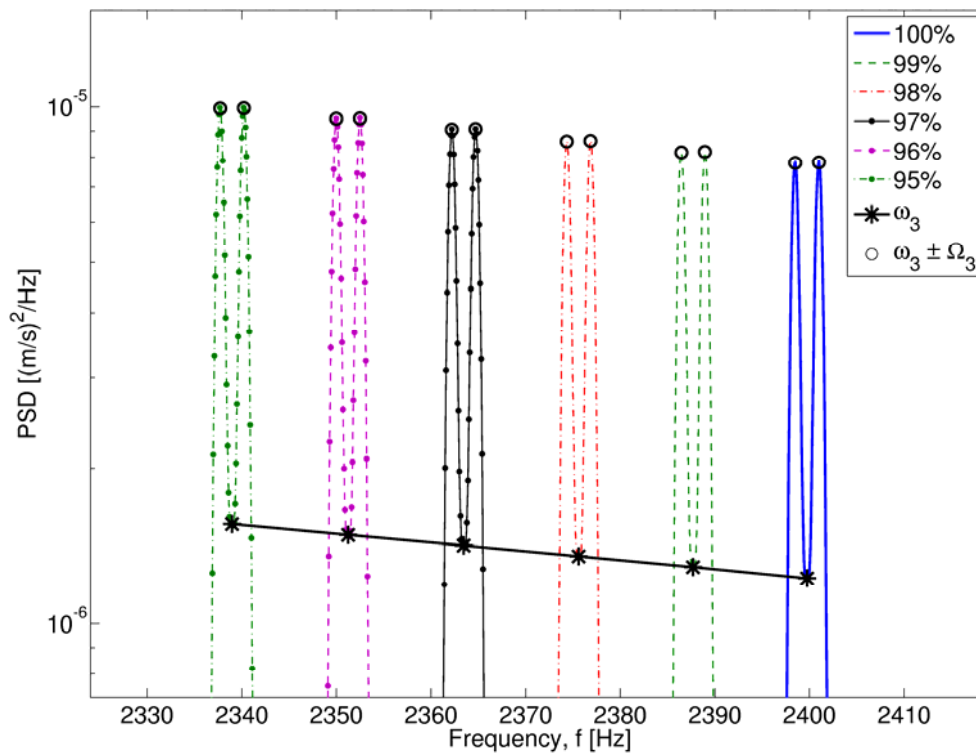


Figure 11: Influence of Young's modulus on EVR PSD around  $\omega_3$

From Figure 11 it is clear that natural frequency shifts can indeed be detected with ELDV, making the measurement approach suitable for condition monitoring purposes. Furthermore it is noted that  $\Omega_3$  remains constant as  $W_3$  is independent of the Young's modulus of the beam. Slight changes can be expected in  $\Omega_j$  when structural damage is considered as this may alter the shape of  $W_j$ .

### 2.3 Experimental study of ELDV

Now that ELDV has been thoroughly studied analytically and numerically, it is desirable to confirm the obtained results experimentally. The verification of Equation 7 was done with the use of a simple test setup that consisted of a cantilever beam mounted with a VibroPet electrodynamic shaker on a chassis running on rails. A load cell was also installed at the excitation point and translation of the chassis was accomplished via a draw wire assembly. This piece of equipment was chosen as it contains a torsional spring which provided an approximate constant pulling force. The draw wire assembly further gave feedback of the chassis position on the rails and the translational velocity of the chassis could subsequently be obtained. The translation speed of the chassis was controlled with the aid of counterweights and out-of-plane vibration of the cantilever beam was measured with an Ometron LDV. The LDV was positioned over a section of the rails where the translation speed of the cantilever beam was approximately constant. Figure 12 shows the experimental setup along with the diagram given in Figure 13.

The natural frequencies and matching mode shapes of the cantilever beam was obtained from static modal testing during which the VibroPet shaker was used for excitation while a Polytec SLDV was used as a transducer. The first six  $\omega_j$ s are listed in Table 3 along with descriptions of the matching mode shapes.

**Table 3: Identified beam natural frequencies**

<i>j</i>	<i>Frequency [Hz]</i>	<i>Description</i>
1	120	1 <sup>st</sup> lateral
2	546	2 <sup>nd</sup> lateral
3	1184	1 <sup>st</sup> torsional
4	1900	3 <sup>rd</sup> lateral
5	6197	4 <sup>th</sup> lateral
6	15090	2 <sup>nd</sup> torsional

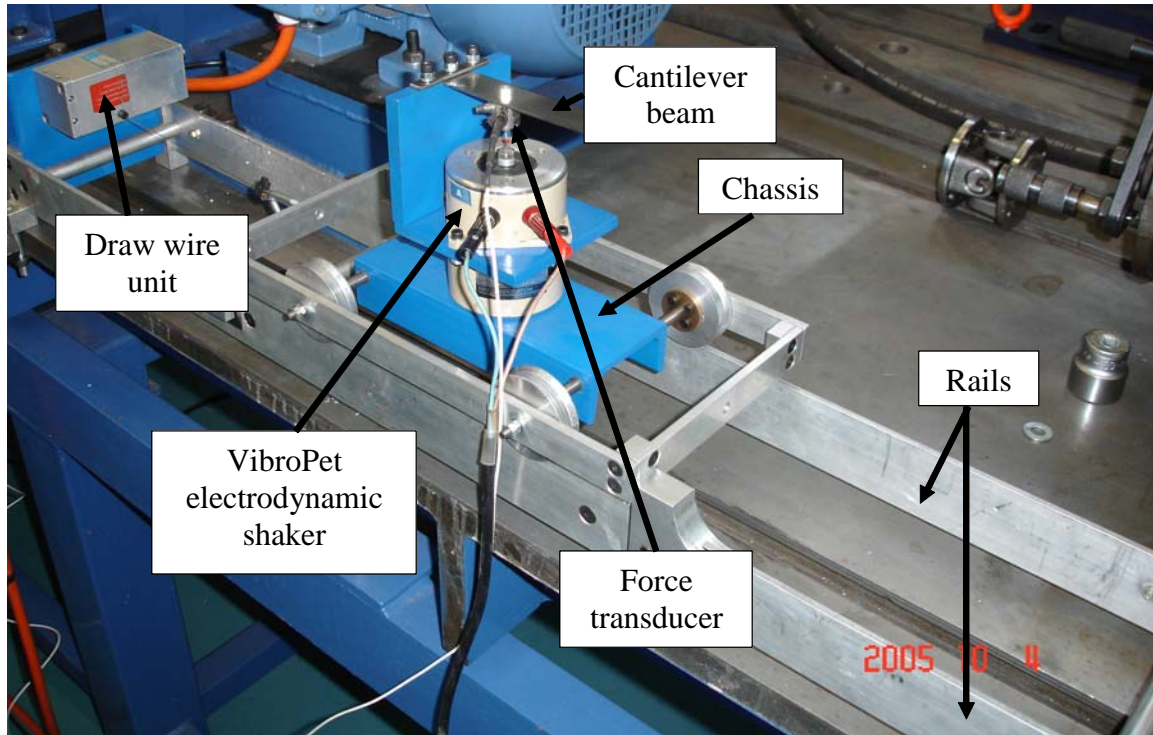


Figure 12: Experimental setup of translating cantilever beam

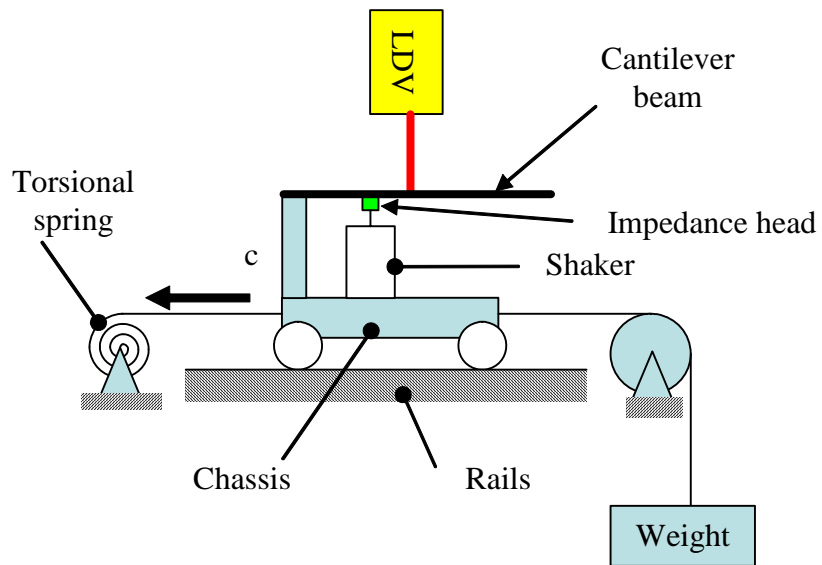


Figure 13: Experimental setup diagram

### 2.3.1 Discrete frequency excitation

To verify the amplitude modulation phenomenon of ELDV, the beam was excited discretely at several frequencies close to its natural frequencies while translating at approximate constant scanning speeds within 3% of 0.463 m/s. Figure 14 shows the EVRs at excitation frequencies of 200 Hz, 500 Hz, 1900 Hz and 6300 Hz. By simple amplitude demodulation of the EVRs by their respective excitation frequencies, the approximate ODSs of the beam are obtained at these frequencies as seen in Figure 14. These ODSs correspond very well with the  $W_{j,s}$  of Figure 8. The discrepancy close to the second nodal point of the ODS at 6300 Hz is present as the excitation location was close to this nodal point. It can also be observed from Figure 14 that the effects of speckle noise become more prominent as the structural response frequencies increase and the response amplitudes decrease accordingly. Since the speckle noise level will remain unchanged at the different frequencies, a decrease in structural response amplitude will result in a reduction of the SNR as is observed from the figure.

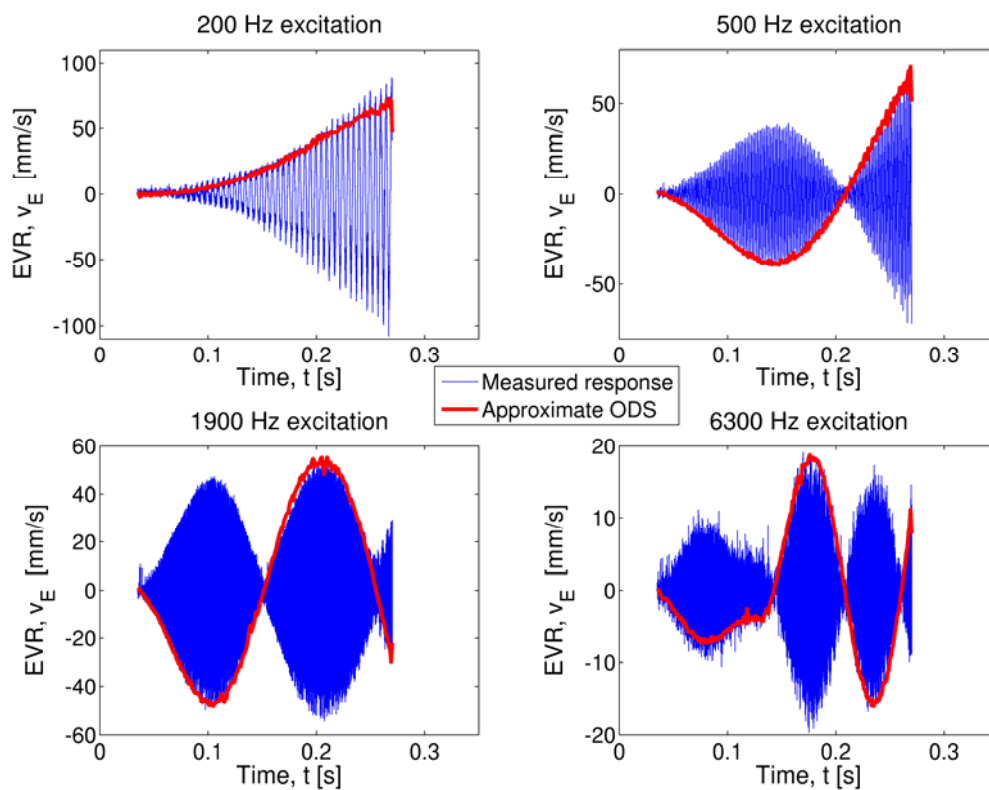
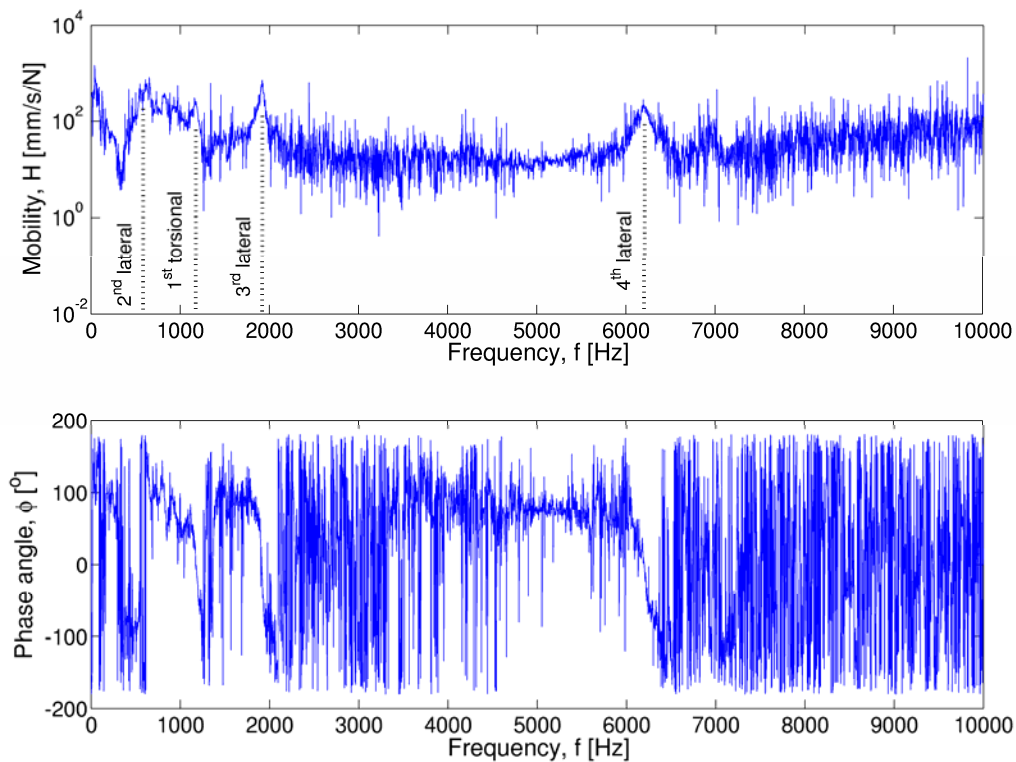


Figure 14: Approximate beam ODSs at discrete frequencies using discrete frequency excitation

The ODSs could also have been obtained by multiplying each EVR with an in-phase and quadrature signal at the relevant excitation frequency (Stanbridge and Ewins, 1999). Modal analysis can furthermore be conducted on these measurements if so required.

### 2.3.2 White noise excitation

Next, to determine whether structural natural frequencies can be identified directly from ELDV measurements, measurements were taken on the test setup using white noise excitation. The scanning speed of the beam was kept within 6 % of 0.539 m/s. Figure 15 depicts the EVR mobility FRF amplitude ( $H$ ) and phase angle ( $\phi$ ) for 25 averages. Several peaks are evident in the FRF amplitude curve in correspondence with phase angle jumps. These peaks correspond well with the identified natural frequencies of Table 3. However, Stanbridge and Ewins (1996) infer that this FRF cannot be used for modal analysis purposes. According to these two authors, sinusoidal scan rates are required for this purpose along with narrow-band excitation. Wideband excitation cannot be used in this application for modal testing purposes as it will result in sideband overlap.



**Figure 15: Spatial averaged frequency response function**

When the time domain measurements are amplitude demodulated in bands of 50 Hz, the average ODSs over these bands can be extracted as shown in Figure 16. The ODSs corresponding to the various mode shapes are clearly visible in the vicinity of the corresponding natural frequencies. The first torsional mode shape exhibits itself as a first bending mode shape as seen from the ODSs in Figure 16 in the vicinity of the beam's first torsional natural frequency.

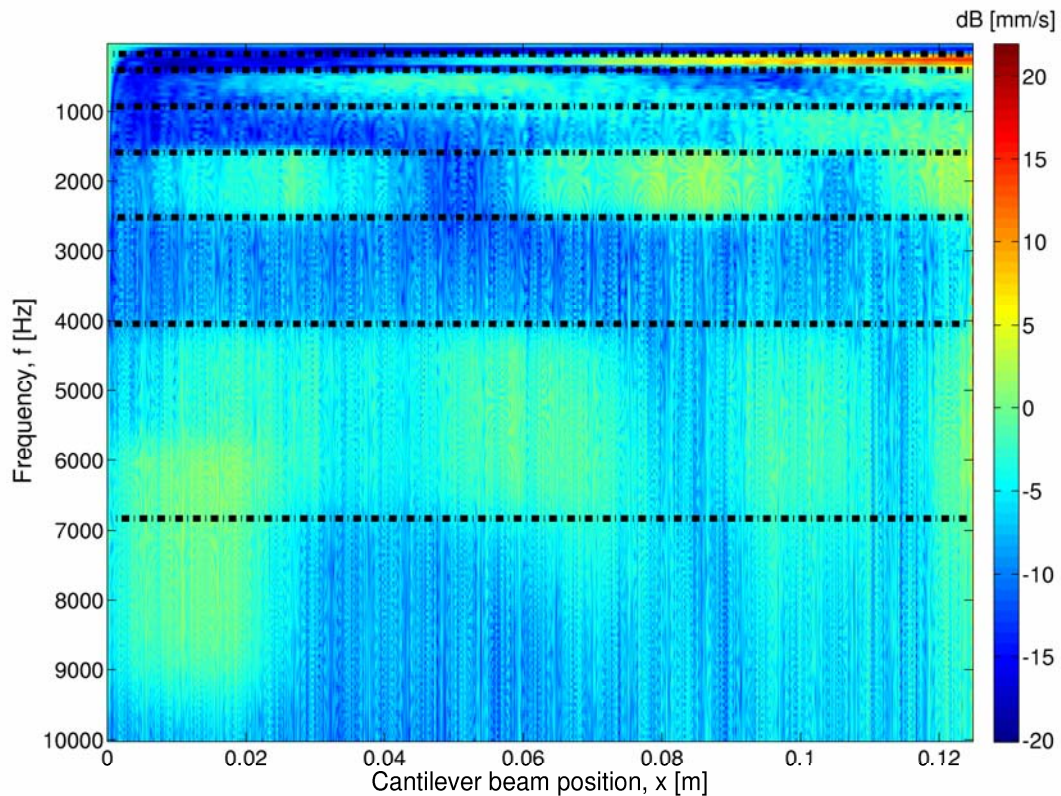


Figure 16: Approximate ODS amplitudes over 10 kHz with white noise excitation

Thus not only can structural natural frequencies be obtained from constant scanning speed ELDV measurements when white noise excitation is employed, but it is also possible to extract ODSs over the entire measurement bandwidth from these measurements.

## 2.4 ELDV on rotating axial-flow blades

Section 2.2 and Section 2.3 were concerned with ELDV on longitudinally translating cantilever beams. In this section, ELDV on rotating axial-flow blades is studied. This can be accomplished by measuring either sideways blade vibration in the rotor-circumferential direction, or flapwise blade vibration in the rotor-axial direction. These two approaches are discussed below.

### 2.4.1 Rotor-circumferential ELDV

With this measurement approach the laser beam is aligned parallel to the rotation plane of the rotor, thereby measuring blade sideways vibration as depicted in Figure 17. However, the ELDV scanning speed will no longer be constant as can be shown

mathematically with the aid of a vector-loop diagram of the measurement setup (Figure 18).

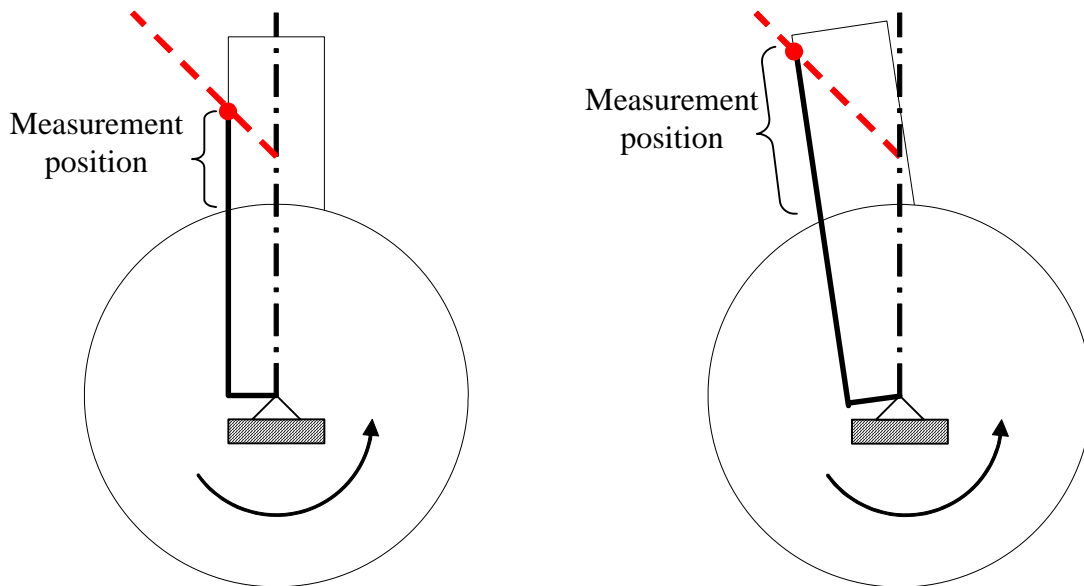


Figure 17: Effect of blade rotation on ELDV measurement position

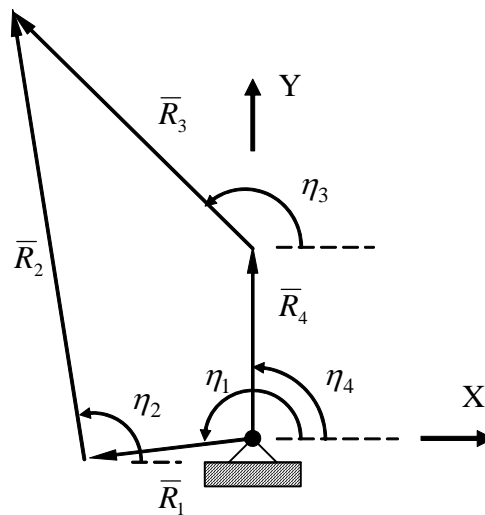


Figure 18: Rotor-circumferential ELDV: Vector-loop diagram

In Figure 18,  $\bar{R}_1$  is defined as the perpendicular vector from the blade leading edge to the rotor centre and  $\bar{R}_2$  describes the ELDV measurement position on the blade leading edge relative to  $\bar{R}_1$ .  $\bar{R}_3$  and  $\bar{R}_4$  describe the laser beam orientation. Using vector-loop equations (Appendix A), it is shown the scan speed  $\dot{R}_2$  is affected by the shaft rotation angle:

$$\dot{R}_2 = \frac{2\dot{\theta}_1 R_1 - \dot{\theta}_1 R_4 \sin \theta_1 - \dot{\theta}_1 R_4 \sin(\theta_1 - 2\theta_3)}{\cos(2\theta_1 - 2\theta_3) + 1}$$

**Equation 19**

It can furthermore be shown analytically and experimentally that this measurement approach introduces a Rigid Body Velocity Component (RBVC) into the measurements. This RBVC  $v_{RB}$  manifests itself as a DC offset in the measurement which depends on the rotor frequency  $\psi$  as well as the LDV orientation:

$$v_{RB} = -2\pi\psi \cdot R_4 \cos \theta_3$$

**Equation 20**

Experimental measurements on a single blade rotor are shown in Figure 19 and a lower limit DC drift can be observed. This phenomenon is most likely caused by the control system characteristics of the SLDV used. Further work is necessary to determine whether this measurement approach is feasible.

## 2.4.2 Rotor-axial ELDV

A simpler approach to perform ELDV on rotating axial-flow blades is to align the LDV parallel to the shaft rotation axis, thereby measuring blade flapwise vibration. In this measurement approach the rotating blade needs to be considered as a cantilever plate undergoing angular translation. Equation 5 and Equation 7 will change to represent the vibration of a plate (Leissa, 1969), whereas the interpolation procedure remains largely unchanged.

To extend the interpolation scheme to a rotating plate, it is convenient to construct a LVRM in a polar coordinate system consisting of LVRs at angular measurement positions  $\varphi_{L,n}$  corresponding to a reference rotor speed  $\psi_{ref}$ :

$$\hat{V}_{L,N_{ref}} = \begin{bmatrix} \bar{v}_{L,\varphi_0} \\ \bar{v}_{L,\varphi_1} \\ \vdots \\ \bar{v}_{L,\varphi_{N_{ref}}} \end{bmatrix} = \begin{bmatrix} v_L(\varphi_0, t_0) & v_L(\varphi_0, t_1) & \cdots & v_L(\varphi_0, t_{N_{ref}}) \\ v_L(\varphi_1, t_0) & v_L(\varphi_1, t_1) & \cdots & v_L(\varphi_1, t_{N_{ref}}) \\ \vdots & \vdots & \ddots & \vdots \\ v_L(\varphi_{N_{ref}}, t_0) & v_L(\varphi_{N_{ref}}, t_1) & \cdots & v_L(\varphi_{N_{ref}}, t_{N_{ref}}) \end{bmatrix}$$

**Equation 21**

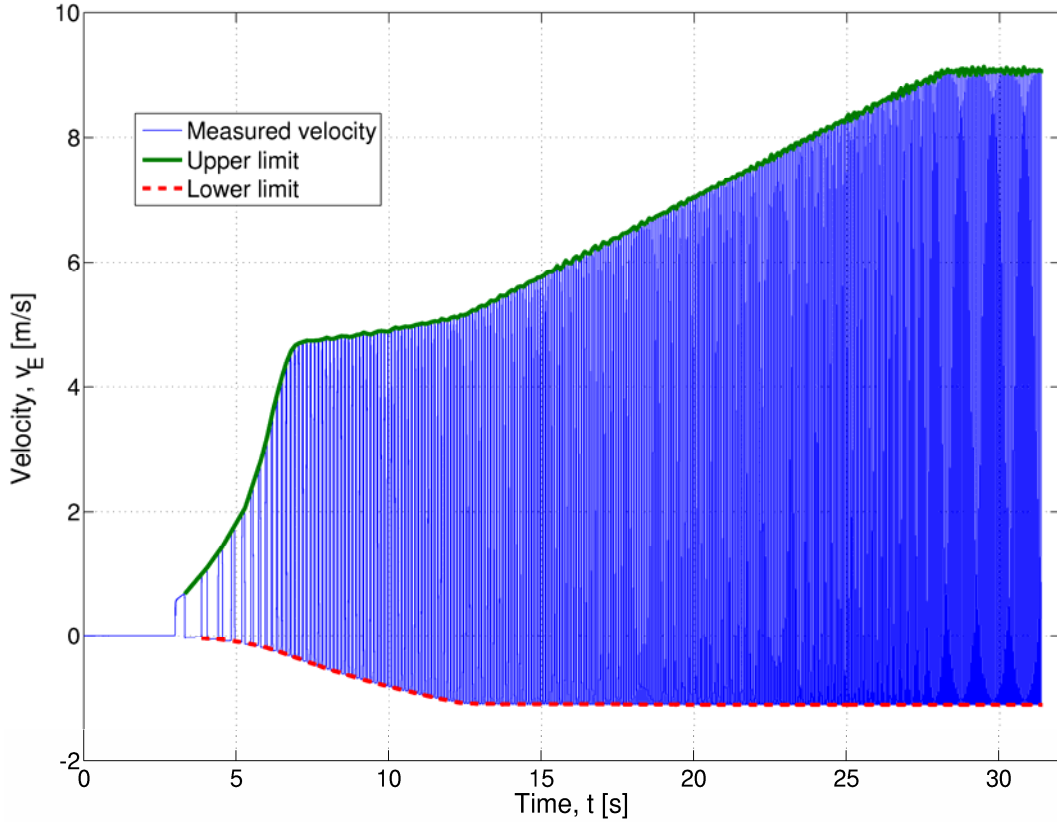


**Figure 19: Rotor-circumferential ELDV: Lower limit DC drift**

with  $\varphi_{L,n} = \psi_{ref} t_n$  and  $N_{ref} = \lfloor \mathcal{G} / (\psi_{ref} \cdot \Delta t) \rfloor$ . The measurement radius is given by  $r$  and the angular measurement range on the blade is represented by  $\mathcal{G}$ .

The polar coordinate EVR vector  $\bar{v}_{E,k,\psi_{ref}}$  can then be obtained at angular positions  $\varphi_{E,n} = k \cdot \omega_{ref} t_n$  by appropriate interpolation on  $\hat{V}_{L,\psi_{ref}}$  for  $k = \psi / \psi_{ref}$  and  $N_k = \lfloor N_{ref} / k \rfloor$  (see Figure 20).

## 2.5 Conclusions

In this chapter, the characteristics of ELDV were studied in depth for longitudinally translating cantilever beams. Using the continuous beam Euler-Bernoulli formulation, it was shown that measurements obtained with ELDV consist of the combined effects of the amplitude modulation of the various cantilever beam generalized coordinates by their respective (and now time-dependent) characteristic functions. This was verified experimentally.

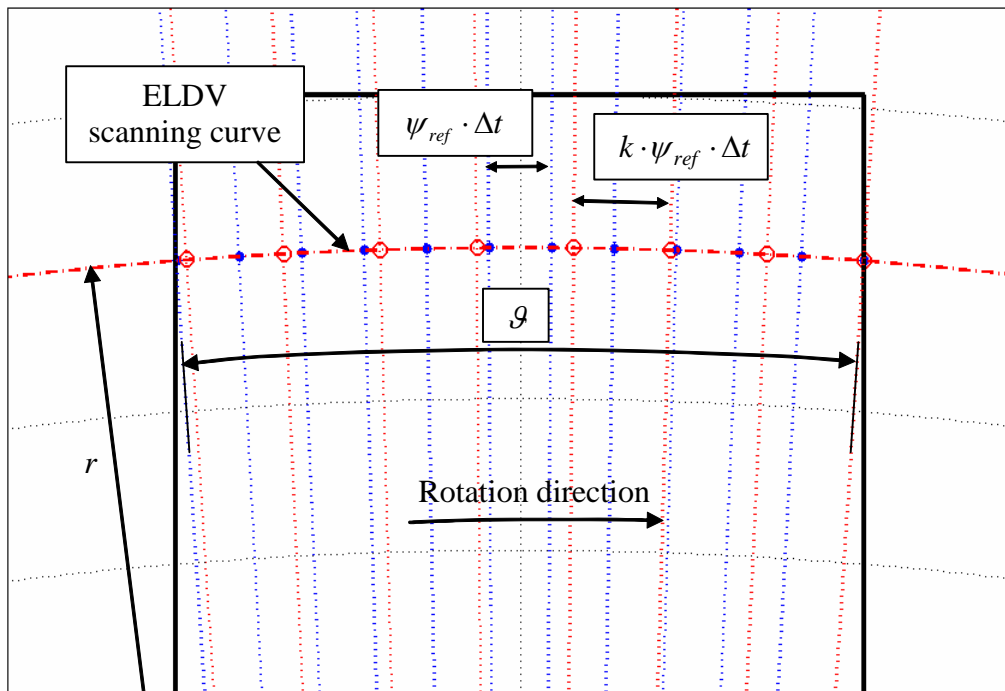


**Figure 20: LVRM and EVR measurement positions for a rotating blade**

The numerical simulation of ELDV was studied next. It was shown that an ELDV signature can directly be obtained from a LVRM when the ELDV scanning speed is an integer multiple of the LVRM scanning speed. When the scanning speed is not an integer multiple, it was shown that the ELDV signature can be approximated accurately with the aid of cubic spline interpolation on the LVRM.

Two approaches for the implementation of ELDV on rotating axial-flow blades were studied namely rotor-circumferential and rotor-axial ELDV. The first approach results in a non-constant ELDV scanning speed and a rotor speed dependent offset is inherent to the measurements. Rotor-axial ELDV however is a much simpler approach as the scan speed remains constant for a fixed rotor speed and no additional components are introduced into the measurements. Using polar coordinates, the interpolation scheme proposed in Section 2.2.3 is easily applied to this measurement approach. It is this measurement approach that this thesis is concerned with.

The work of this chapter is summarized in the article titled “*Online condition monitoring of axial-flow turbomachinery blades using rotor-axial Eulerian laser Doppler vibrometry*” (Oberholster and Heyns, 2009).